

AD 711085



AD

AMMRC CR 70-14

**INVESTIGATION OF THE APPLICATION OF COHERENT ACOUSTIC
IMAGING TO NONDESTRUCTIVE TESTING**

April 1970

W. R. Arndt and J. L. Kreuzer
The Perkin-Elmer Corporation
Optical Group, Research
Norwalk, Connecticut

Semi-Annual Technical Report - Contract DAAG46-69-C-0010

This document has been approved for public release and sale; its distribution is unlimited.

Prepared for

**ARMY MATERIALS AND MECHANICS RESEARCH CENTER
Watertown, Massachusetts 02172**

Reproduced by the
CLEARINGHOUSE
for Federal Scientific & Technical
Information Springfield Va. 22151

ACCESSION FOR	
CPST	WHITE SECTION <input checked="" type="checkbox"/>
DDG	BUFF SECTION <input type="checkbox"/>
UNAN.	CED. <input type="checkbox"/>
JUSTIFICATION	
BY	
DISTRIBUTION/AVAILABILITY CODES	
DIST.	AVAIL. CODE or SPECIAL
<input checked="" type="checkbox"/>	

The findings in this report are not to be construed as an official Department of the Army position, unless so designated by other authorized documents.

Mention of any trade names or manufacturers in this report shall not be construed as advertising nor as an official indorsement or approval of such products or companies by the United States Government.

DISPOSITION INSTRUCTIONS

Destroy this report when it is no longer needed.
Do not return it to the originator.

AMMRC CR 70-14

**INVESTIGATION OF THE APPLICATION OF COHERENT ACOUSTIC IMAGING
TO NONDESTRUCTIVE TESTING**

W.R. Arndt and J.L. Kreuzer
The Perkin-Elmer Corporation
Optical Group, Research
Norwalk, Connecticut

April 1970

Semi-Annual Technical Report - Contract DAAG46-69-C-0010
Sponsored by
Advanced Research Projects Agency
ARPA Order No. 1245
Program Code No. 19D10

This document has been approved for public release and sale; its distribution is unlimited.

Prepared for

ARMY MATERIALS AND MECHANICS RESEARCH CENTER
Watertown, Massachusetts 02172

TABLE OF CONTENTS

<u>SECTION</u>	<u>TITLE</u>	<u>PAGE</u>
I	INTRODUCTION	1
	A. Background	1
	B. Technical Goals	1
	C. Summary of Progress	2
	D. Program For Next Six Months	2
II	ULTRASONIC HOLOGRAPHIC CAMERA	4
	A. Theory of Operation	4
	B. Hardware Development	20
	C. Experimental Results	43
III	ULTRASONIC DIFFRACTION MICROSCOPE	48
	A. Theory	48
	B. Experiments	53

LIST OF ILLUSTRATIONS

<u>FIGURE</u>	<u>TITLE</u>	<u>PAGE</u>
1	Ultrasonic Holographic Camera (Recording)	5
2	Ultrasonic Holographic Image Reconstruction (Imaging)	5
3	Recording an Acoustic Hologram of the Internal Structure of a Metal Block	7
4	Actual Hologram of a Long Hole in an Aluminum Block	8
5	Images Formed from Figure 4 Using Two Different Imaging Techniques (Image Plane Parallel to Hologram vs Parallel to Hole)	8
6	Functional Block Diagram - Ultrasonic Holographic Camera Recorder	10
7	Point Images as a Function of the Recording Point Spread Function	16
8A	Point Images as a Function of Range For Short Gates	17
8B	Point Images as a Function of Gate Durations	19
9	Block Diagram - Ultrasonic Holographic Camera	22
10	Photograph of New Timer Unit	23
11	Block Diagram of New Timer Unit	24
12	Timing Diagram of New Timer Unit	25
13	Schematic Diagram-Receiver Preamp Unit	27
14	Schematic Diagram - Receiver Mixer/Amplifier	28
15	Timing Diagram - Gated Integrator	30
16	Schematic Diagram - Gated Integrator	31

LIST OF ILLUSTRATION (continued)

<u>FIGURE</u>	<u>TITLE</u>	<u>PAGE</u>
17	Timing Diagram - Light Modulator	33
18	Schematic Diagram - Light Modulator	34
19	Waveform Photographs	36
20	Waveform Photographs	36
21	Waveform Photographs	37
22	Waveform Photographs	38
23	Waveform Photographs	38
24	Experimental Set-up for Measuring Flatness of the X-Y Scanning Plane	40
25	Single Line Profile Across the Scanning Plane (5 μ Peak-to-Peak)	41
26	Composite Profile Across the X-Y Scanning Plane (5 μ Peak-to-Peak)	41
27	"Grating-Effect" in Artificial Acoustic Hologram due to Velocity Modulation in the X-Y Scanning Plane	42
28	Block Diagram - New Mechanical Scanner	44
29(a)	Processed Signal from Hole in Block, Revised System (10- μ sec Transmitted Pulse)	45
29(b)	Processed Signal from Hole in Block, Revised System (2 - μ sec Transmitted Pulse)	45
30	Hologram of 1.6 MM Diameter Aluminum Wire, Revised System (10- μ sec Transmitted Pulse)	47
31	Reconstructed Image of 1.6 MM Diameter Aluminum Wire, Revised System	47

LIST OF ILLUSTRATIONS (continued)

<u>FIGURE</u>	<u>TITLE</u>	<u>PAGE</u>
32	Bragg Angle Imaging Relations	49
33	Schematic Diagram - Lens Ultrasonic Diffraction Microscope	54
34	Photograph - Spherical Lens Ultrasonic Diffraction Microscope	56
35	Light Intensity Distribution in Diffraction Plane of Ultrasonic Diffraction Microscope	56
36	Schematic Diagram - Mirror Ultrasonic Diffraction Microscope	57
37	Photograph - Mirror Ultrasonic Diffraction Microscope	58

SECTION I

INTRODUCTION

A. BACKGROUND

This report is the second semi-annual Technical Report on Contract No. DAAG46-69-C-0010 with the U.S. Army Materials and Mechanics Research Center in Watertown, Massachusetts, and covers the period 1 May 1969 through 31 October, 1969. This contract concerns a research program whose purpose is to analyze and perform experimental demonstrations of the application of ultrasonic holographic and ultrasonic light diffraction techniques to the detection, analysis, and examination of the internal structure of optically opaque materials. The program is funded by the Advanced Research Projects Agency, Washington, D.C.

The research program under this contract covers the period from November 1968 through June 1970, and follows the work accomplished by Perkin-Elmer during 1965-1968 under Contract Nos. DA-19-066-AMC-286(X) and DAAG46-67-0132(X). Under these earlier contracts Perkin-Elmer demonstrated the feasibility of the holographic technique in forming three-dimensional acoustic images of solid objects and their internal structure. The results of that work are published in the contract technical reports and in references (1) and (2).

B. TECHNICAL GOALS

Recommendations made upon completion of Contract No. DAAG46-67-0132(X) were the technical goals pursued under the present contract. These goals were as follows:

- (1) Mechanical and electrical revision of the ultrasonic holographic camera in order to remove mechanical imperfections in the scanning system and electronic drift associated with the breadboard receiver and data processor.
- (2) Production of new acoustic holograms and the formation of images therefrom with the revised and renovated ultrasonic holographic camera.
- (3) Fabrication of an ultrasonic diffraction microscope for the purpose of forming images directly from acoustic-optic interactions.

C. SUMMARY OF PROGRESS

The work accomplished during the period covered by this report included the following:

- (1) The complete redesign, fabrication, and test of the ultrasonic holographic camera.
- (2) The redesign of the mechanical scanner for the ultrasonic holographic camera.
- (3) The production of ultrasonic holograms with the new ultrasonic holographic camera, and the analysis of the images produced.
- (4) The fabrication of the ultrasonic diffraction microscope and the analysis of the images produced by the acoustic-optic interaction within this device.

Because of the extensive time required for redesign, fabrication and testing of the new ultrasonic holographic camera, it was not possible to incorporate the mechanical redesign by installing the new motor drives into the scanner. The design of these drive mechanisms is complete, however, and fabrication has been started, so that it should be possible to make the conversion soon.

Due to the extensive system redesign, it also was not possible to construct and analyze as many holographic images as had been planned. However, with the inherent flexibility, improved stability, and enhanced performance expected from the revised system, it is anticipated that rapid progress can be made during the next contract interval in accomplishing this work.

D. PROGRAM FOR NEXT SIX MONTHS

The ultrasonic holographic camera has been completely redesigned and rebuilt to provide greater flexibility and more stable operation; all that remains in its modification is the substitution of the new scanner motor drives. Therefore, it is expected that a considerable portion of the next six-month interval can be devoted to the generation of holograms and their subsequent reconstruction and evaluation. Toward this goal, a series of tests have been planned which image the internal structure of test specimens through a range of transmitted pulse widths, receiver range-gate intervals, and other parameter variations.

In addition to the generation and analysis of the holographic images, specific tasks to be accomplished during the next interval include:

- (1) Installation of the new scanner motor drives.
- (2) Investigation of the use of different operating frequencies with the ultrasonic holographic camera.

- (3) Investigation of receiver-transducer arrays and sampling techniques for use in examination of the internal structure of materials.
- (4) Investigation of optical filtering to improve interpretation of imaging from the internal structure of materials.

An elementary theory of the ultrasonic diffraction microscope is outlined in this report and some preliminary supporting experiments are described. This work will now be used to design a direct-imaging real-time ultrasonic diffraction microscope suitable for imaging the interior of solids. To achieve this goal, the following tasks will be undertaken during the next six months:

- (1) We will re-examine cylindrical line-source imaging techniques to compare them more carefully to spherical point-source imaging techniques. A more detailed theory of line-source and point-source imaging techniques will be developed.
- (2) We will make a preliminary study of the differences between the imaging of the exterior of objects in water and the interior of objects with the diffraction microscope. It is suspected that the imaging of the interior of objects will require range gating, solid diffraction cells, and higher frequencies.
- (3) Some ultrasonic diffraction microscope images will be made and analyzed.

SECTION II

ULTRASONIC HOLOGRAPHIC CAMERA

A. THEORY OF OPERATION

1. General

Basically, a hologram is a recording which, when illuminated from a monochromatic point source (i.e., a source of radiation which is both temporally and spatially coherent), reacts with the illuminating radiation in such a way as to create a multiplicity of new wavefronts corresponding both in strength and apparent source position to all points in the scene which was recorded. This is the operation which has been called "wavefront reconstruction."³ In order for a hologram to reconstruct wavefronts, it is necessary that the hologram store data on both the phase and amplitude of all wavefronts originally emanating from the coherently-illuminated scene being holographed.

If suitably carried out, there is no restriction in holography as to the type of radiation chosen for creating the hologram, nor to the type of radiation used for illuminating the hologram in performing wavefront reconstruction. Thus, synthetic aperture radar holograms are made of the surface of the earth with microwave radiation. These holograms, when illuminated by means of coherent light, reconstruct wavefronts which may be perceived by the human eye. Thus, images of the two dimensional radar scattering properties of the earth may be visually observed and/or recorded. In an exactly similar fashion, holograms may be recorded using coherent sound waves and then utilized to perform wavefront reconstruction in the visible. Here the viewer sees an image whose intensity corresponds to the three dimensional scattering properties of an object originally "illuminated" by coherent sound. Because of the fact that sonic radiation propagates in many materials which are opaque to light, acoustic holography provides us with an opportunity to "look inside" these materials and see their internal structure.

An example of one method of forming a synthetic aperture acoustic hologram is shown in Figure 1.⁴ Here a block of material containing a localized acoustic scattering center or "hole" is illuminated by means of coherent sound. The scatterer produces a spherical wave emanating in all directions. This spherical wave may be picked up by a transducer scanning in an acoustically flat plane. If the output of this transducer is connected to a homodyne detector operating at the original acoustic frequency, then it is possible to detect both the amplitude and phase of the scattered sound. To record the acoustic hologram, a small lamp is made to mechanically track the scanning transducer. The emission

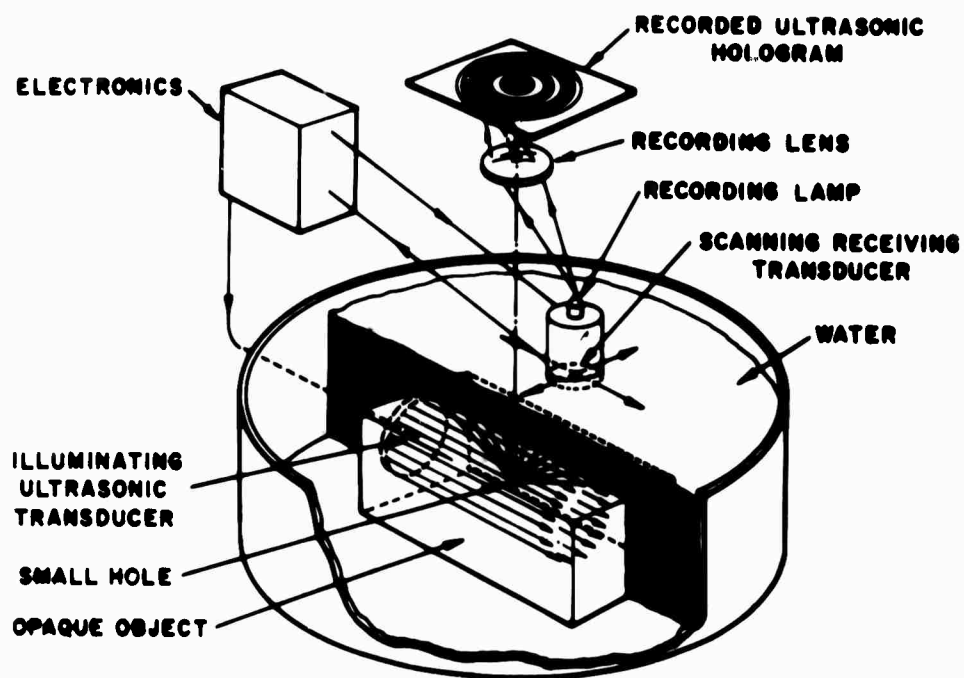


Figure 1. Ultrasonic Holographic Camera (Recording)

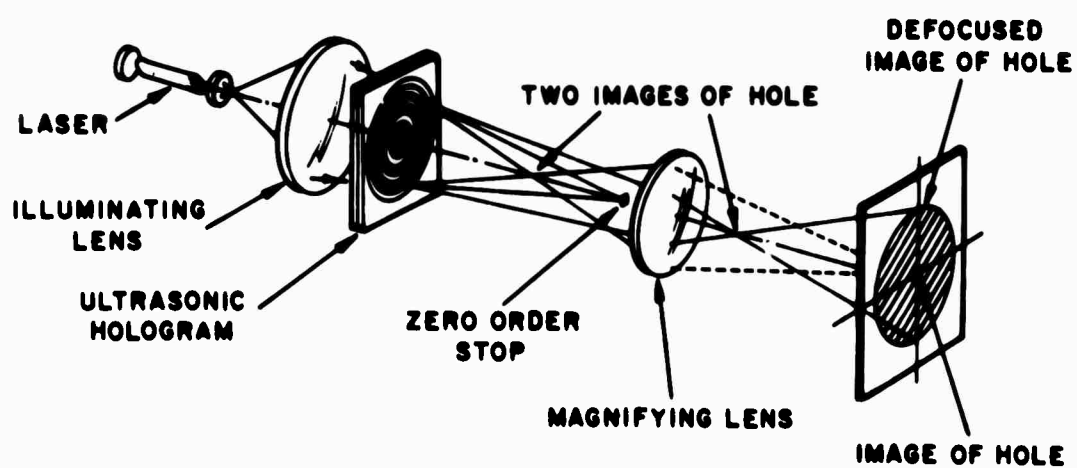


Figure 2. Ultrasonic Holographic Image Reconstruction (Imaging)

from the lamp is made to correspond on a point-by-point basis to the product of the sonic field amplitude with the cosine of the detected phase angle. When this is done for a point scatterer of sound (Figure 1), the resultant acoustic hologram is the well-known Fresnel zone plane.^{5,6}

The apparatus shown in Figure 2 shows how a hologram of a point scattering center may be used to reconstruct the original wavefront and, therefore, produce an image of the point scatterer which can be seen visually. The hologram is placed in a beam of coherent optical radiation (here produced by a laser). The zone plate has lens-like properties which cause it to focus some of the incident light to a point. A wavefront converging to a point is, of course, spherical and is the reconstruction (now by electromagnetic energy of optical wavelength) of the original acoustic wavefront. This optical wavefront produces a point image which may be viewed by an observer or recorded on photographic film. Note that the zone plate also reconstructs a diverging spherical wavefront yielding a second, or "virtual," image of the point scatterer. In acoustic holography light associated with the virtual image appears strongly defocused in the plane of the real image and thus does not create an objectionable effect. Light which is not influenced by the hologram is removed from the imaging system by means of what is called a "zero order stop" (see Figure 2).

An example of acoustic holography illustrating its use in analyzing the internal structure of an object is shown in Figure 3. Here a long slanted hole has been formed in an aluminum block. When coherent energy impinges on the hole, it is scattered and picked up by the scanning transducer. The type of hologram which results is shown schematically in Figure 3. An actual hologram made of an 8-cm long, one millimeter diameter hole in an aluminum block is shown in the upper portion of Figure 4. If this hologram is properly scaled in the recording process by the ratio of the acoustic wavelength used for holographing to the optical wavelength used for wavefront reconstruction, then the image produced at the optical wavelength would focus along a tilted line, now having a length in optical wavelengths as long as the original hole in acoustic wavelengths.

For an acoustic frequency of five megahertz, and a wavelength (in aluminum) of approximately 2 millimeters, the image of the hole is only 40 optical wavelengths long, or about 20 microns. Thus, the visible image formed is microscopic. As we view this image through the microscope we find that we have the usual depth-of-focus problems characteristic of any low f-number imaging system. This is amply illustrated in the left-hand image in Figure 5, which shows the holographic image of the slanted hole viewed at the upper end. As can be seen, only a portion of the image is in focus, whereas most of the image of the hole is in an extremely defocused position. In an attempt to solve the focusing problem, an experiment has been performed wherein the viewing optical system was tilted so as to lie in the plane of the image of the hole. The resultant image is shown in the right-hand position of Figure 5, demonstrating how the image of the entire hole may be viewed at once.

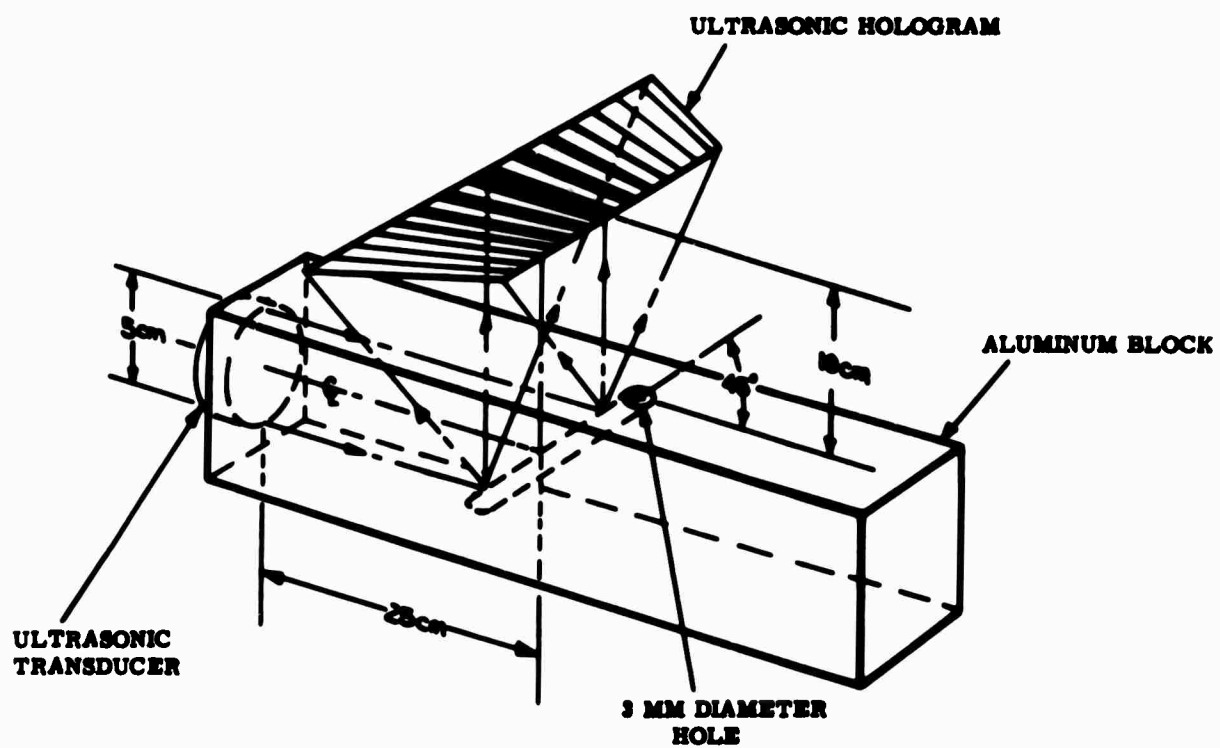


Figure 3. Recording an Acoustic Hologram of the Internal Structure of a Metal Block



Figure 4. Actual Hologram of a Long Hole in an Aluminum Block

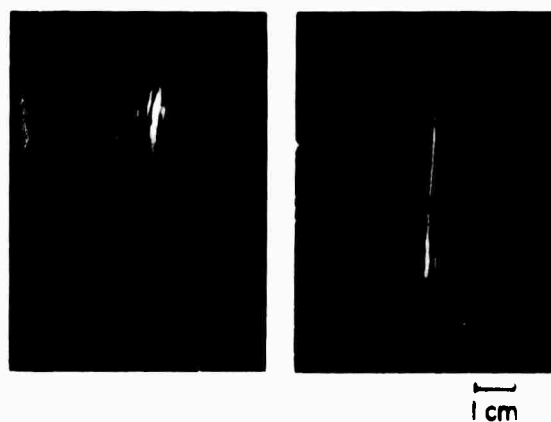


Figure 5. Images Formed from Figure 4 Using Two Different Imaging Techniques (Image Plane Parallel to Hologram vs Parallel to Hole)

2. Sampled Holograms

a. Hologram Recording

The ultrasonic hologram formed using the ultrasonic holographic camera is "range-gated", i.e., it is temporally sampled to eliminate undesired ultrasonic reflections such as those from the surfaces of the specimen and from the walls of the tank which contains the specimen. Without range-gating these reflections were observed to completely mask scattering from the interior of the specimen. Range-gating produces a temporally and hence also a spatially sampled ultrasonic hologram.

The following assumptions and notation are made to simplify this analysis. These assumptions do not appreciably reduce the applicability of the results.

- (1) The analysis is presented in two dimensions.
- (2) The transmitting and receiving transducers are assumed to be at the same location (i.e., scanning together). We expect to modify our system to do this, because it appears to be the best way to scan a large area uniformly.
- (3) Phase and amplitude changes that are a function of the acoustic angle of incidence are ignored. The effect of these changes requires further study.
- (4) The hologram reference is "on axis" (the hologram scan plane is the referenced phase plane). Later we may move the reference off axis.
- (5) Acoustic attenuation due to energy absorption and spreading, and obliquity factors are ignored.
- (6) Undefined constants will be denoted by C_i for $i = 0, 1, 2, \dots$ as needed.
- (7) Numerical subscripts on voltages (V) refer to the points marked on Figure 6.
- (8) The subscript l stands for the l^{th} pulse. τ will be used for variable time durations, and T for fixed time durations

The optical field transmittance $a_o(x)$ of an ideal ultrasonic hologram can be written as a weighted sum of sinusoidal zone plates. Each such zone plate of the sum can be written as

$$a_o(x) = C_o + C_1 \cos w_o \tau \quad (2-1)$$

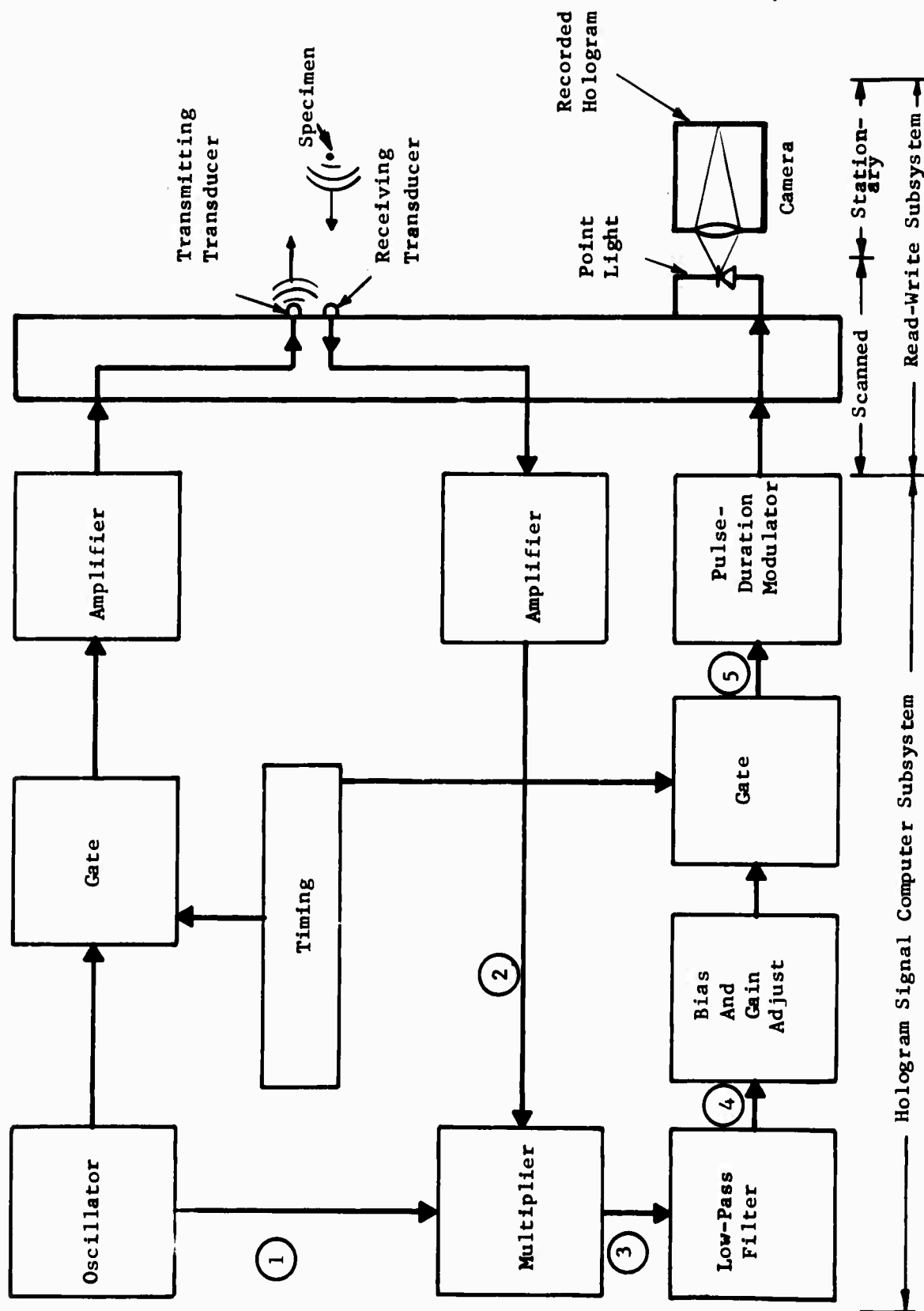


Figure 6. Functional Block Diagram - Ultrasonic Holographic Camera Recorder

where ω_0 is the ultrasonic temporal frequency and

$$\tau = 2V^{-1}(x^2 + z^2)^{1/2} \quad (2-2)$$

is the time required for an ultrasonic pulse to travel at the velocity v from the transmitting transducer to an ultrasonic point scatterer and return to the receiving transducer. The spatial coordinates are (x, z) . The point scatterer is located at $(0, 0)$. The hologram plane (line) is a distance $z \gg 0$ away from the point scatterer and parallel to the x axis.

The temporally sampled holograms are recorded to produce a spatially sampled optical field transmittance $a_1(x)$ of the following form

$$a_1(x) = \sum_{\ell} (b_{\ell} + C_2) s(x - x_{\ell}) \quad (2-3)$$

where b_{ℓ} is the hologram sample produced by pulse number ℓ of L pulses; C_2 is a bias constant that satisfies the condition $b_{\ell} + C_2 > 0$ in order to keep the optical field transmittance positive; $s(x - x_{\ell})$ is the recording point-spread function, or spatial optical field transmittance produced by the recording light exposure and includes the effect of the recording camera optics on the hologram centered at the point $x = x_{\ell}$.

The ultrasonic hologram camera recorder computes the hologram sample b_{ℓ} by the following operations:

The electrical reference voltage is

$$V_1 = \cos \omega_0 t \quad (2-4)$$

where t is time. The output voltage of the receiving transducer amplifier in response to ultrasonic pulse number ℓ can be written as the product

$$V_{2,\ell} = f(t - \ell T_1 - \tau_{\ell}) \cos \omega_0 (t - \tau_{\ell}) \quad (2-5)$$

where $f(t)$ is the "received pulse envelope function", including phase, at the output of the ultrasonic receiver transducer amplifier, and T_1 is the time between pulses. The ultrasonic pulse propagation delay is τ_{ℓ} , in analogy to Equation (2-2). In order to record a satisfactory hologram we require that $f(t)$ be band-limited to frequencies less than ω_0 (i.e., have no energy for temporal frequencies greater than the ultrasonic temporal frequency). The received pulse envelope function includes the transmitted ultrasonic "pulse" frequencies as received through the temporal frequency response of the receiving transducer and the electrical amplifiers which follow. Only the composite envelope function is important.

Next we form the "heterodyne" product of the reference and the amplified received ultrasonic signal

$$V_{3,\ell} = V_1 V_{2,\ell} \quad (2-6)$$

The low-pass filter temporally filters $V_{3,\ell}$ to retain temporal frequencies less than the ultrasonic frequency, but included in the band-limited received pulse envelope function. The filtered voltage $V_{4,\ell}$ can be idealized as the convolution integral

$$V_{4,\ell} = \int V_{3,\ell}(t-u) \frac{\sin \omega_0 u}{\pi u} du \quad (2-7a)$$

$$= f(t - \ell T_1 - \tau_\ell) \cos \omega_0 \tau_\ell \quad (2-7b)$$

We then adjust the gain, and add a bias to expose the photographic film over a linear range. We will ignore the gain and bias at this point.

We time gate the voltage $V_{4,\ell}$ to accomplish ultrasonic range gating which eliminates undesired echoes. The result of this time gating is

$$V_{5,\ell} = V_{4,\ell} g(t - \ell T_1 - T_2) \quad (2-8)$$

where $g(t)$ is the multiplicative receiver temporal gate function, and T_2 is the receiver delay time (separation between the transmitted pulse and the receiver gate function).

The ultrasonic hologram sample b_ℓ (and hence exposure) is proportional to the time integral of the voltage $V_{5,\ell}$. Our actual exposure is given by a constant brightness for a time proportional to b_ℓ , plus the bias constant. The exposure time for the ℓ^{th} hologram sample is

$$\tau_{1,\ell} = C_3 \int V_{5,\ell}(t) dt + C_4 \quad (2-9a)$$

$$= C_3 h_\ell \cos \omega_0 \tau_\ell + C_4 \quad (2-9b)$$

where

$$h_\ell \equiv \int f(t + T_2 - \tau_\ell) g(t) dt \quad (2-9c)$$

and

$(T_2 - \tau_\ell)$ is the time difference between the ultrasonic pulse propagation delay time and the receiver gate delay time.

The correlation function (h_ℓ) is (the integral of) the coincidence time between the received ultrasonic pulse, which occurs at the varying ultrasonic pulse propagation delay times τ_ℓ as the transducers scan, and the fixed receiving delay gate time function. Equation (2-9c) shows that the role of the received pulse envelope and the receiver gate functions are interchangeable, and that the time between pulses, T_1 , need not be constant from pulse to pulse.

The sampled hologram optical field transmittance can be written by combining Equations (2-3) and (2-9b) to yield a recorded zone plate transmittance of

$$a_1(x) = \sum_{\ell} (C_2 + C_5 h_\ell \cos w_o \tau_\ell) s(x - x_\ell). \quad (2-10)$$

This can be seen to be essentially a sampled version of the continuous sinusoidal zone plate given by Equation (2-1), except for the gate coincidence function (h_ℓ) which causes part (or all) of the zone plate to be absent if the received pulse envelope and gate functions do not coincide. It is normally desirable for h_ℓ to be a "smooth function." That is, the magnitude of the Fourier transform of h_ℓ should be small for frequencies greater than the reciprocal duration of h_ℓ . This means that both the received pulse envelope and the receiver gate function also should be smooth functions. The requirement for h_ℓ to be a smooth function will be apparent from the next section on image formation.

b. Image Formation

The visible image is formed by placing the recorded hologram transparency with the optical field transmittance given by Equation (2-10) in the optical system shown in Figure 2. We will discuss the effect of sample spacing (x_ℓ) in a later report. For now we will let the sample spacings be very small and equal, so that the sum in Equation (2-10) becomes the convolution integral

$$a_2(x) = \int (C_2 + C_5 h(u) \cos w_o \tau) s(x - u) du \quad (2-11a)$$

where Equation (2-9c) is replaced by

$$h(x) = \int f(t - T_2 - \tau) g(t) dt \quad (2-11b)$$

and τ is a function of x ($x = u$ in Equation (2-11a)). Equation (2-11a) can be written in complex notation as

$$a_2(x) = a_3(x) + a_3^*(x) + C_6 \quad (2-12)$$

where the star (*) denotes the complex conjugate, and

$$a_3(x) \equiv C_7 \int h(u) e^{j w_o \tau} s(x - u) du. \quad (2-13a)$$

We can expand the exponent as

$$w_0 \tau \approx C_8 + u^2 B \quad (2-13b)$$

where

$$B \equiv \frac{w_0}{vz}. \quad (2-13c)$$

The real image is formed by $a_3(x)$, the virtual image by $a_3^*(x)$, and the zero order by C_6 . In the appropriately scaled focal plane, the real image intensity $i(x)$ is given by the square of the optical field $u(x)$.

$$u(x) = \int a_3(v) e^{-jBv^2} e^{jvx} dv \quad (2-14a)$$

and

$$i(x) = |u(x)|^2. \quad (2-14b)$$

Equations (2-13a) through (2-14b) can be combined to yield

$$u(x) = C_9 \int H(x-2Bv) s(v) e^{j(xv-Bv^2)} dv \quad (2-15)$$

where

$$h(x) \longleftrightarrow H(v) \quad (2-16)$$

are a Fourier transform pair.

We can neglect the phase term in Equation (2-15) because in a well-designed system, both $H(v)$ and $s(v)$ are non-zero only for $v \approx 0$. This is true because the desired spatial extent of $h(x)$ is large and $s(x)$ small. This leads to the following two forms for the image optical field:

$$u(x) = C_{10} \int H(x-v) s\left(\frac{v}{2B}\right) dv \quad (2-17a)$$

$$= C_{11} \int h(w) S(2Bw) e^{jwx} dw \quad (2-17b)$$

We will discuss Equations (2-17a) and (2-17b) in some detail. The extent of the zone plate is determined by the spatial extent of the gate co-incidence function $h(x)$. Equation (2-17a) gives the optical field image as the convolution of the scaled recording point-spread function and the Fourier transform of the zone plate extent. Equation (2-17b) gives the optical field image as the Fourier transform of the product of the zone plate extent and the Fourier

transform of the scaled recording point-spread function. It is common to call $u(x)$ the coherent point-spread function. The Fourier transform $U(w)$ of $u(x)$ (where x and w are the Fourier transform variables, and w is the radian spatial frequency) is called the coherent modulation transfer function. From Equation (2-17b) we see that the coherent modulation transfer function is $h(w_x)S(2Bw_x)$.

The extent of $u(x)$ is small for a high resolution image. This implies that $h(x)$ should be a smooth function (as previously defined) of large extent, and $s(x)$ small in extent to record a zone plate of uniformly high modulation over a large extent. Once the extent of $s(x)$ is small enough there is no gain in making it smaller. However, $s(x)$ should not be too small, or we will reduce the linear dynamic range of the photographic record of the hologram because the dynamic range of the film is a function of the area exposed. The detailed nature of $s(x)$ will be discussed in a later report in conjunction with the effect of sample position.

Figure 7 shows the decrease in resolution for too large a recording point-spread function. The low resolution image (a) when $s(x)$ is too large extent is the image produced by a zone plate lens of smaller diameter than the zone plate for $s(x)$ of smaller extent (b).

Next, we will examine the point image as a function of $h(x)$ for $s(x)$ sufficiently small to achieve high resolution. To do this we will approximate $s(x)$ by a delta or impulse function, so that Equation (2-17b) becomes

$$u(x) = C_{11} \int h(w) e^{jwx} dw \quad (2-18)$$

Figure 8A shows the effect of identical short gates [$f(t) = g(t)$]. Short gate times are times much less than the receiver delay line T_2 . The corresponding spatial extent of $f(t)$ and $g(t)$ are shown. Five acoustic point scatters are shown at various distances from the receiving transducer. The receiver delay is optimized for the cross-hatched region centered at point (c). The gate coincidence function $h(x)$ for these five points determines the fraction of the energy used to record the zone plate, as shown. Sound propagating within the marked angles is recorded. No hologram is recorded from point (a), because a real transducer will accept only sound within a certain acceptance angle (its antenna radiation pattern). The sound from (a) that corresponds to the non-zero values of $h(x)$ is not recorded (shown as dashed lines), because the sound is assumed to be outside this acceptance angle. The three zone plates recorded (b,c,d) form images (at the appropriate distance) as shown magnified below their respective acoustic points. These images are enlarged and exaggerated to emphasize their different diffraction detail. These three points are the conventional point images for:

Example b - a conventional apodized or shaded zone plate lens with a large central obscuration. It exhibits high resolution with large amplitude side lobes.

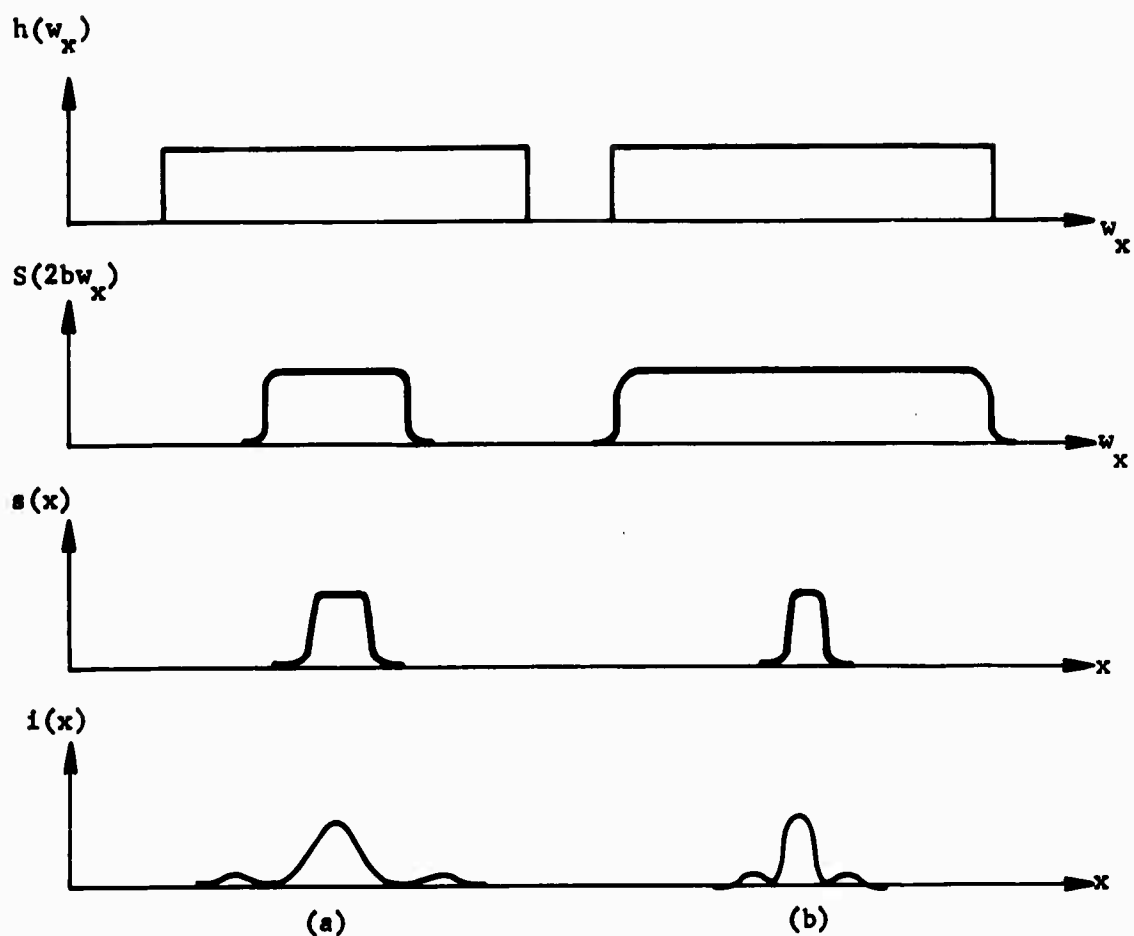


Figure 7. Point Images as a Function of the Recording Point-Spread Function

- (a) Poor resolution caused by a recording point-spread function of too large an extent.
- (b) Better resolution not limited by the recording point spread function.

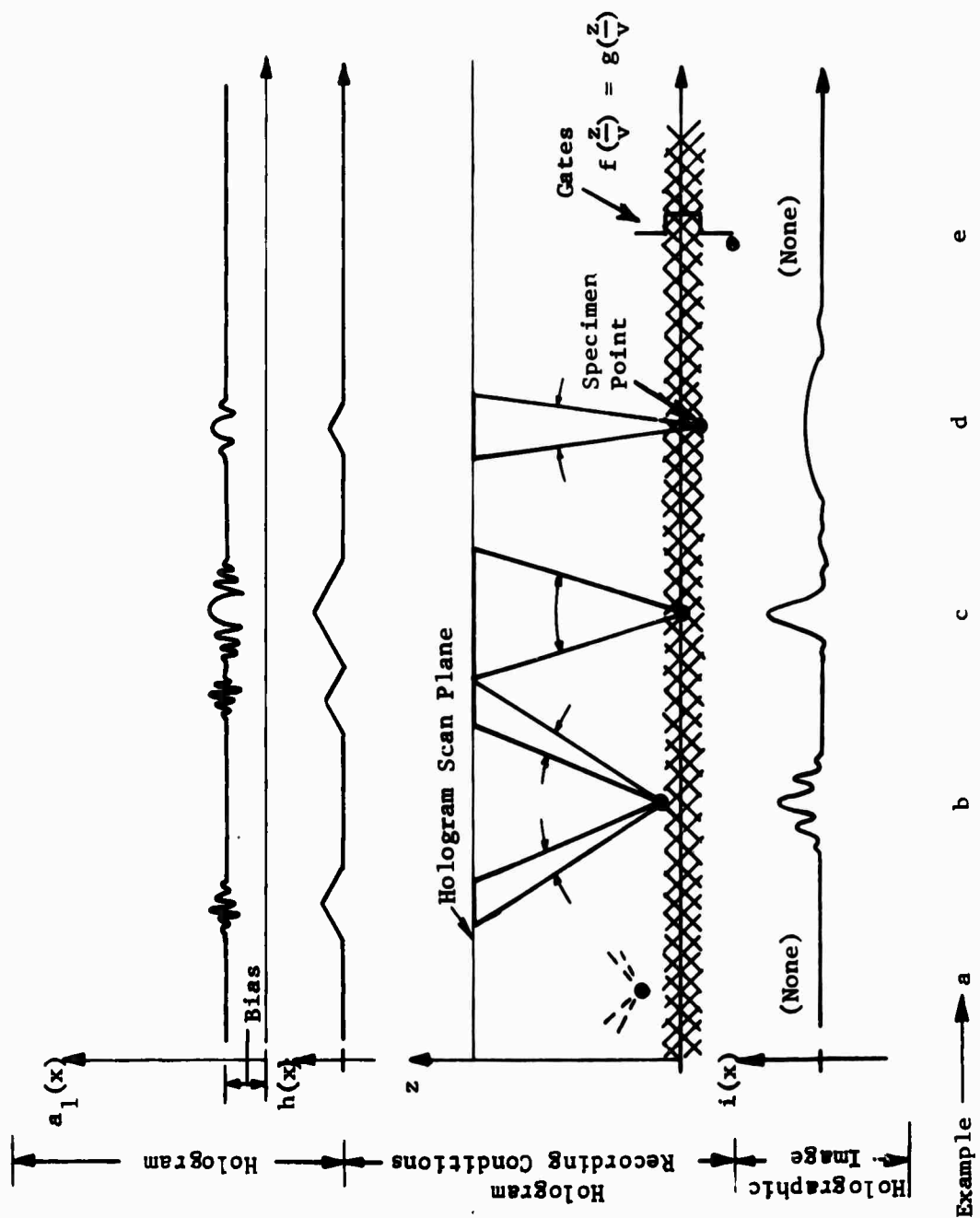


Figure 8A. Point Images as a Function of Range For Short Gates

Example c - A conventional apodized zone plate lens. It exhibits high resolution with small amplitude side lobes.

Example d - A conventional apodized zone plate lens of small extent. It exhibits low resolution.

Figure 8B shows images as a function of the received pulse envelope duration and the receiver gate duration for a point centered in the receiver gate. All other variables are held constant. The three cases show:

Example f - both gates short. It exhibits low-resolution image.

Example g - either gate short and the other gate long. It exhibits a high-resolution image with side lobes, typical of a conventional zone plate lens.

Example h - both gates long. It exhibits a brighter high-resolution image with low amplitude side lobes, typical of an apodized zone plate lens.

The actual choice of available gate durations depends upon sample geometry and location, echo isolation and signal-to-noise considerations. Acoustic dispersion and attenuation inside a sample with high attenuation and/or scatter could be an important factor in some cases. A more detailed basis for the selection of gate durations must await further experimentation.

c. Summary

This section has described a simple set of parameters that yields a satisfactory holographic image. There is a fair degree of freedom in the detailed design of the system described. Certain other systems will also yield satisfactory ultrasonic holograms. At this time, these other variations seem to offer no apparent advantage. Violations of the conditions described to record a temporally sampled ultrasonic hologram will generally result in an inferior ultrasonic holographic image. The image may be degraded in two general ways (1) linearly and (2) nonlinearly.

Linear degradations include errors such as phase shifts and amplitude weighting over the hologram zone plates. In principle, linear degradation can be corrected in the recorded hologram by the use of inverse linear holographic spatial filtering, but one would like to avoid this. Factors which can contribute to linear degradation arise from all portions of the system, including the electrical circuits, the optical paths and the photographic film. Two areas requiring further study are (1) the amplitude and phase transmittance as a function of the acoustic angle of incidence through the water-to-specimen interface, and (2) the transmitting-receiving transducer phase and amplitude response as a function of angle.

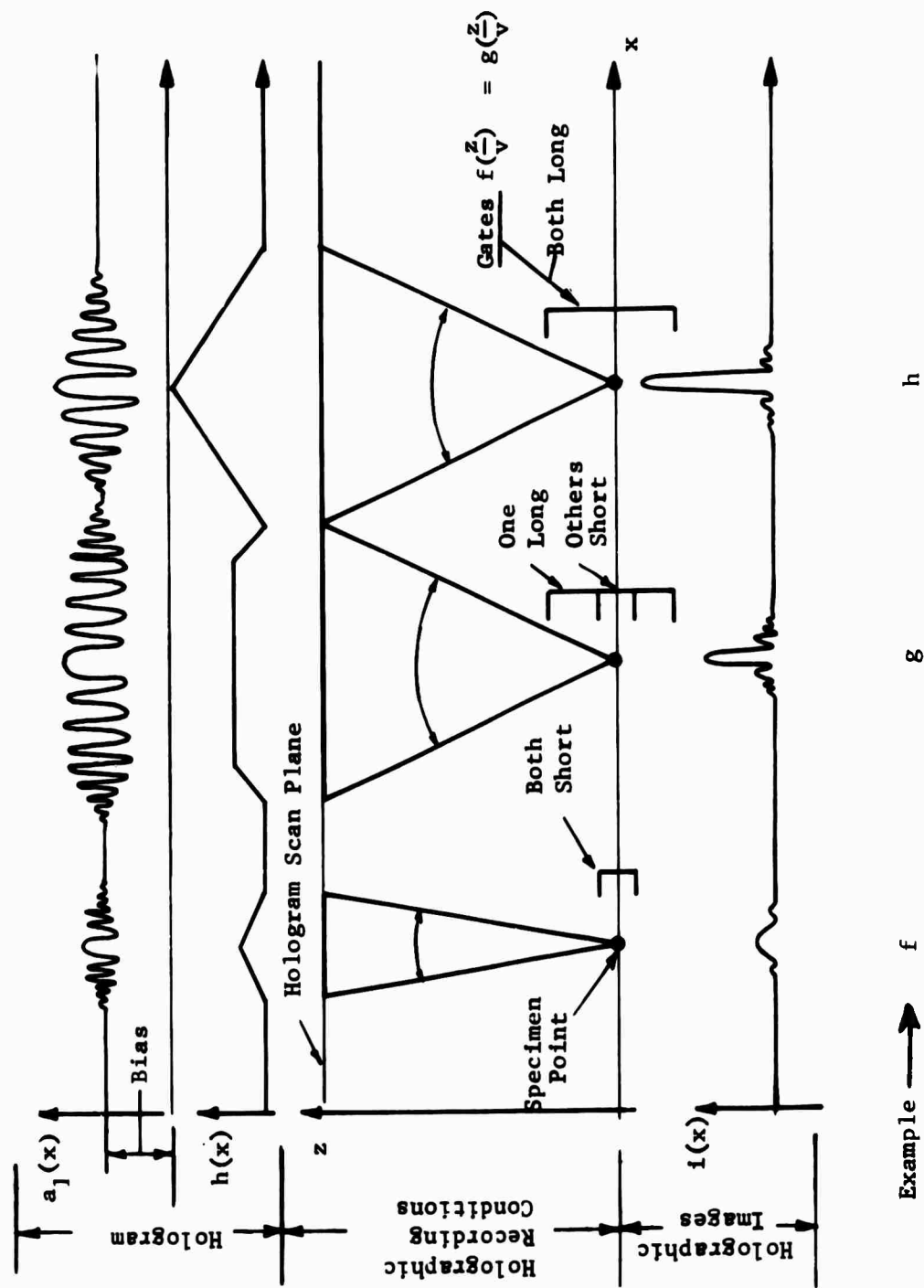


Figure 8B. Point Images as a Function of Gate Durations

Nonlinear degradation is not correctable, in general. However, nonlinear degradation can be considered within two classes: (1) nonlinearities uncorrelated to the desired hologram signals, and (2) nonlinearities correlated to the desired hologram signal. Basically, uncorrelated nonlinearities add a random background, or noise, to the image, while correlated nonlinearities add a nonrandom background. Nonlinearities correlated with the image are most undesirable.

There are many nonlinear system degradations which can affect overall system performance. It is important that the basic set of system parameters outlined earlier not be violated, and that excessive noise, time-dependent parameter changes (drift), electrical nonlinearities, limited dynamic range, photographic nonlinearities, and mechanical scanner motion irregularities be minimized.

Design tolerances for linear and nonlinear degradation factors are difficult to specify because of the lack of detailed ultrasonic holographic image data. However, these data are currently being collected. In the absence of this detailed information, conventional optical tolerances have been used for linear and nonlinear degradation tolerances. In this regard, the tolerances for correlated nonlinearities have caused the most difficulty. Often, very rigid initial conditions are assumed to be necessary. This leads to design tolerances that cannot be met, but the system works anyway. Although the original design tolerances are clearly too rigid, it is not known how much, or in which direction, they can be relaxed. Further ultrasonic holographic image experience should reduce this uncertainty of the design tolerances. For this reason, the linearity and noise properties of our system should be measured.

B. HARDWARE DEVELOPMENT

1. General

In the original ultrasonic holographic camera, the processing of the received and reference signals to produce a hologram (according to the theory outlined in the last section) was accomplished by summing, squaring, and adding a constant (bias) before integrating, range-gating and modulating the recording light. Although theoretically sound, the analogue operations required to instrument this approach were difficult to implement without introducing nonlinearities, scale factor changes, instabilities and long-term drifts. Although of no consequence in the production of holograms, the system also was not completely coherent, the phase of the carrier frequency (5 MHz) being completely random with respect to each transmitted pulse. It was difficult in such a system to maintain the proper timing relationships when transmitter pulse widths, pulse repetition rates and other parameters were changed.

By using the carrier frequency (5MHz) as the master timing waveform, the entire system can be made phase coherent, and a much simpler implementation used. The summing and squaring operations are replaced by simple coherent mixing (multiplication), and the constant added by controlling the average brightness of the recording light. This is the basic implementation of the new transmitter and receiver-processor design.

A fundamental block-diagram of the new system is shown in Figure 9. The timer unit generates all of the gating waveforms and synchronizes the entire system. The transmitter gates a portion of the 5 mHz carrier frequency and amplifies the pulsed carrier to drive the transmitting transducer. The receiving transducer is integral with its preamplifier, and is mounted on the carriage of the scanner.

The receiver multiplies the received signal by the 5 mHz reference signal, filters the mixed output, and integrates a selected portion of the returned signals. The output of the receiver is a dc voltage proportional to the integral of the multiplied signals. This voltage is used by the light modulator to control the "on time" of a pulsed light-emitting diode, also mounted on the scanner carriage. More detail will now be provided on the individual blocks of Figure 9.

2. Timer

A photograph of the new timer unit is shown in Figure 10, and a block diagram in Figure 11. The unit provides timing signals for the entire system which are phase-locked to the carrier frequency of the transmitted pulses. (Although a 5 mHz carrier frequency is being used for present tests, other frequencies can be used by changing the crystal oscillator and retuning the transmitter.) Convenient thumb switches on the front panel permit instant change of pulse repetition rate, transmitter pulse width, and receiver gate start and stop times.

In the block diagram of Figure 11 the oscillator input is first "squared" by means of a shaping circuit. The output of the shaper is divided by 5 and used to drive a 6-stage decade counter whose outputs are used to generate four basic timing intervals. These timing intervals are:

- (1) the transmit period;
- (2) the transmit gate;
- (3) the received delay; and
- (4) the received gate.

Each of these four basic timing intervals are generated by means of comparators which are fed from both the decade counter, and from Digiswitches mounted on the panel of the timer unit. The transmit gate, received delay, and received gate may be varied in steps of 1 microsecond (presently 5 cycles of the oscillator output) to 9,999 microseconds, i.e., there are three Digiswitches for use in selecting each of these intervals. This transmit period may be varied between one microsecond and 999,999 microseconds. The longest transmit period yields a lowest repetition frequency of approximately 1 Hz.

When each comparator reaches a match with the output of the decade counter, a flip-flop, which is set at the start of the repetition interval, is reset, thus terminating the corresponding time interval. In order to generate the receive gate, the outputs of the transmit gate and the receiver delay are used to provide inputs to an AND circuit. A timing diagram for the timer unit is shown in Figure 12. Note that the phase of the pulsed transmitter carrier is coherent from pulse to pulse.

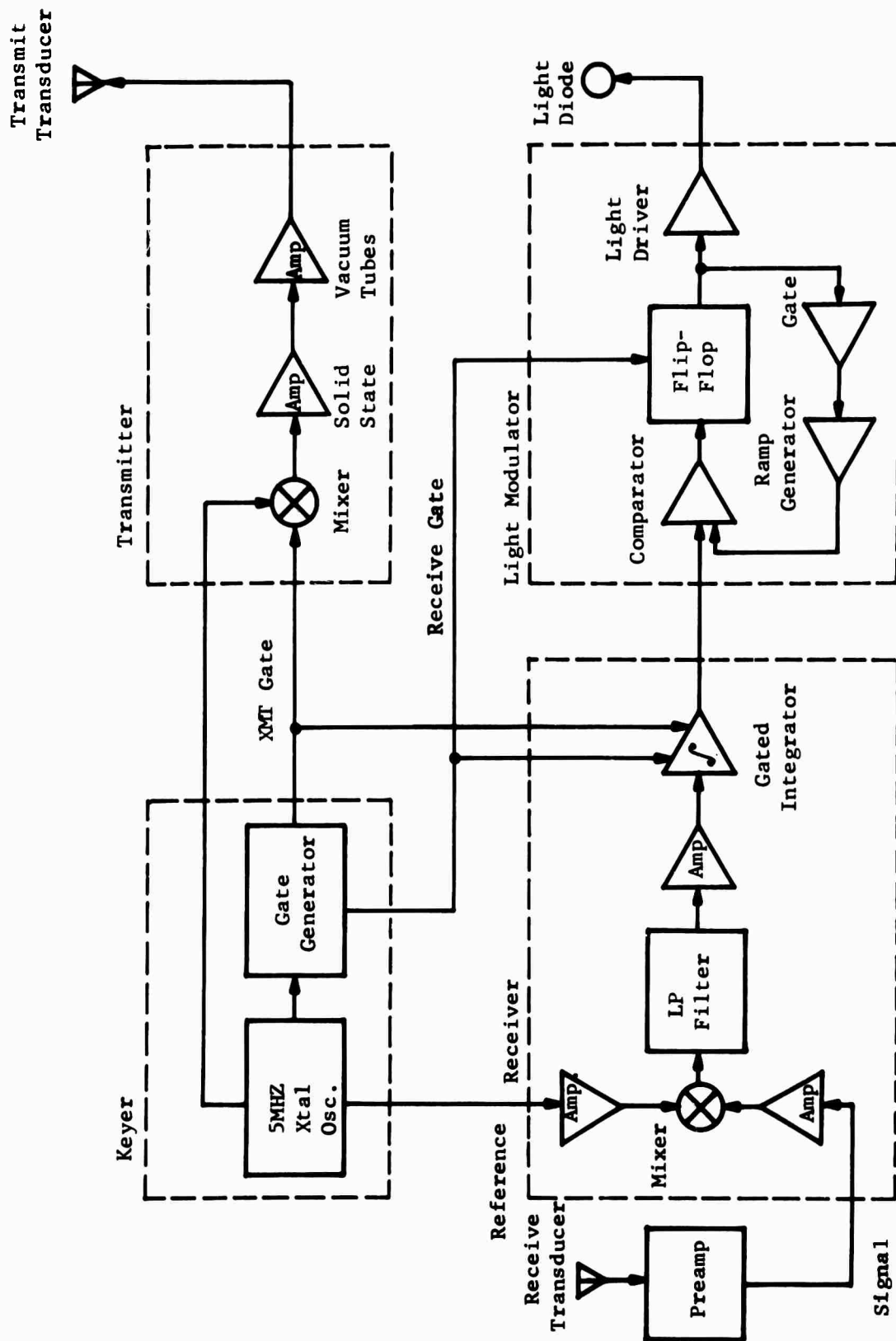


Figure 9. Block Diagram - Ultrasonic Holographic Camera

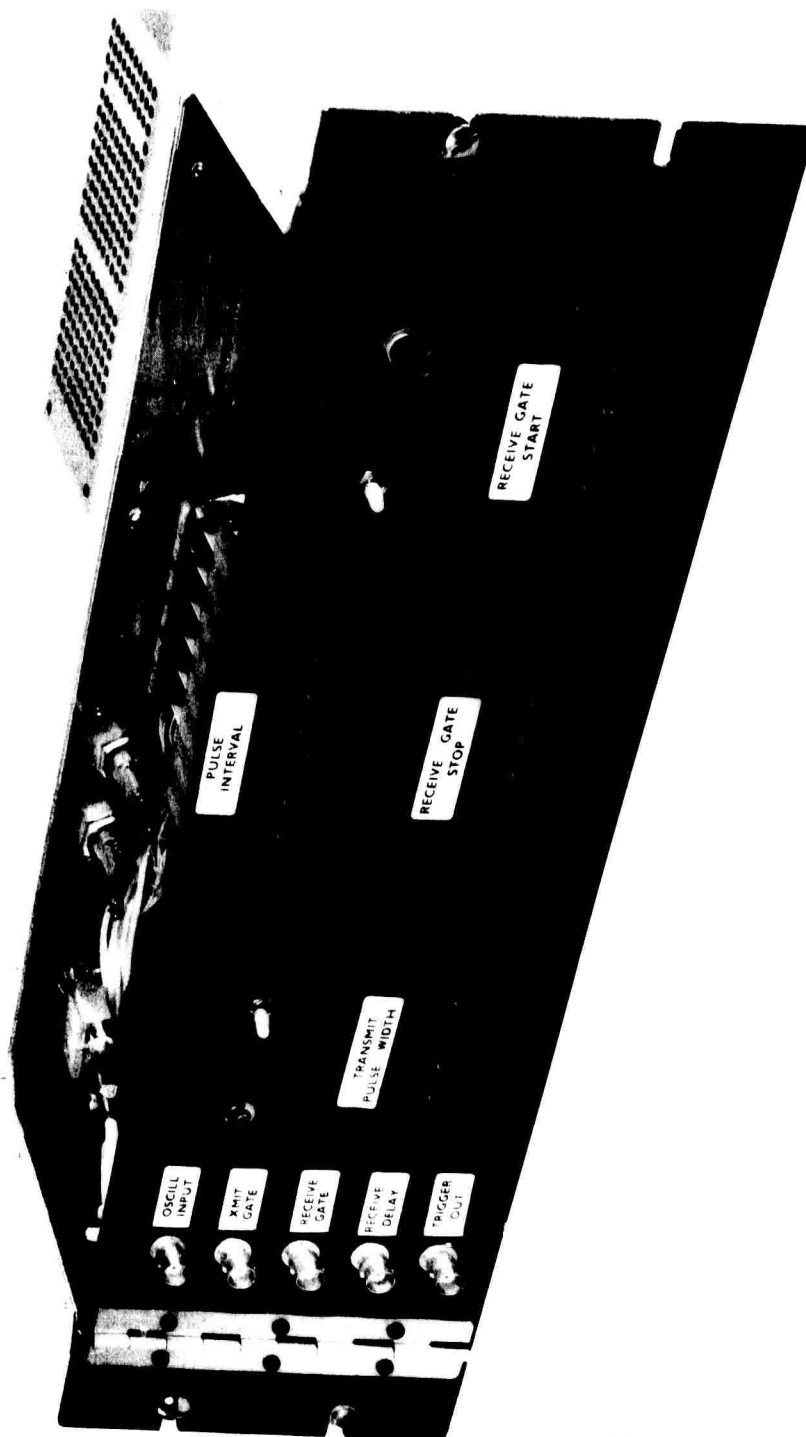


Figure 10. Photograph of New Timer Unit

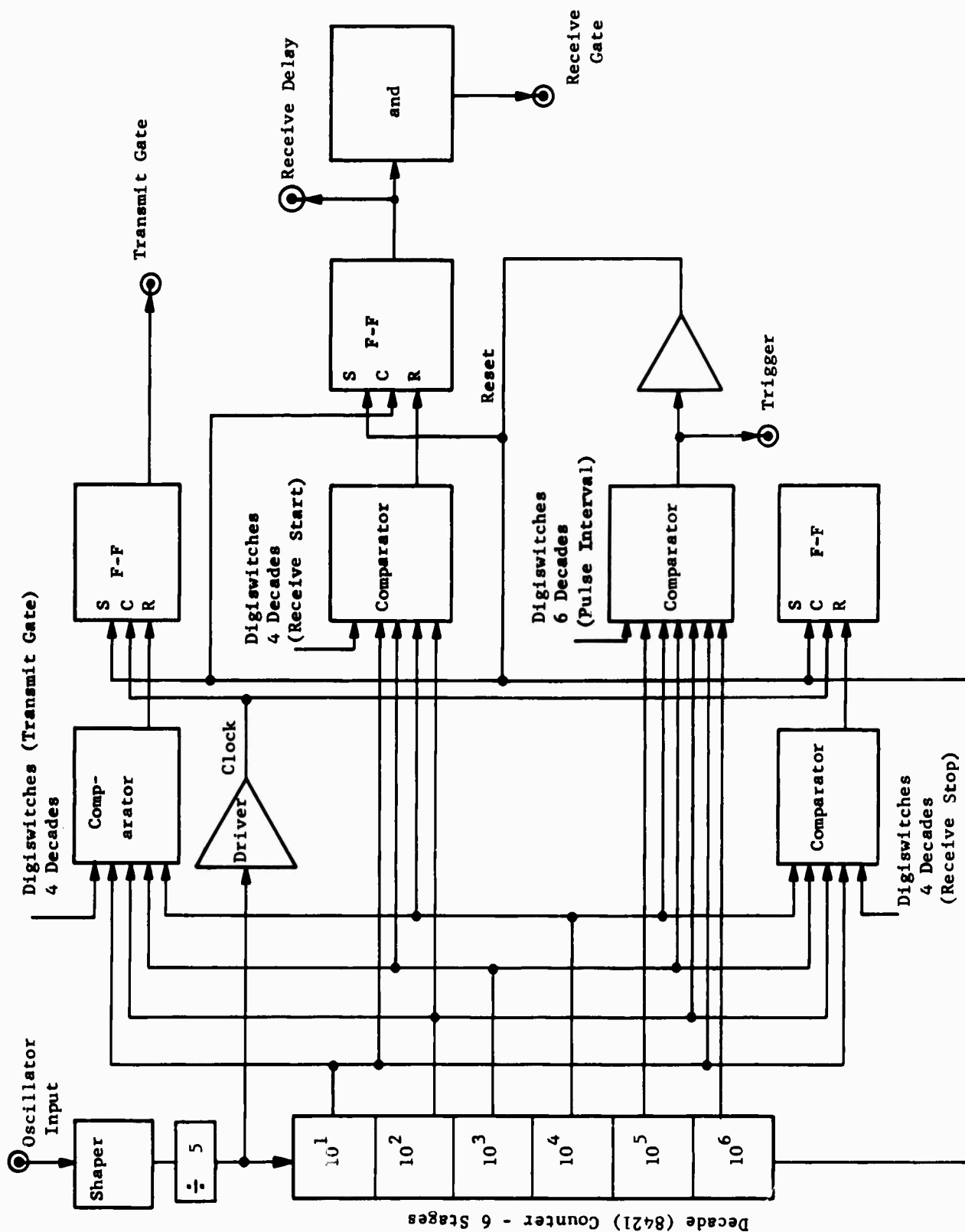


Figure 11. Block Diagram of New Timer Unit

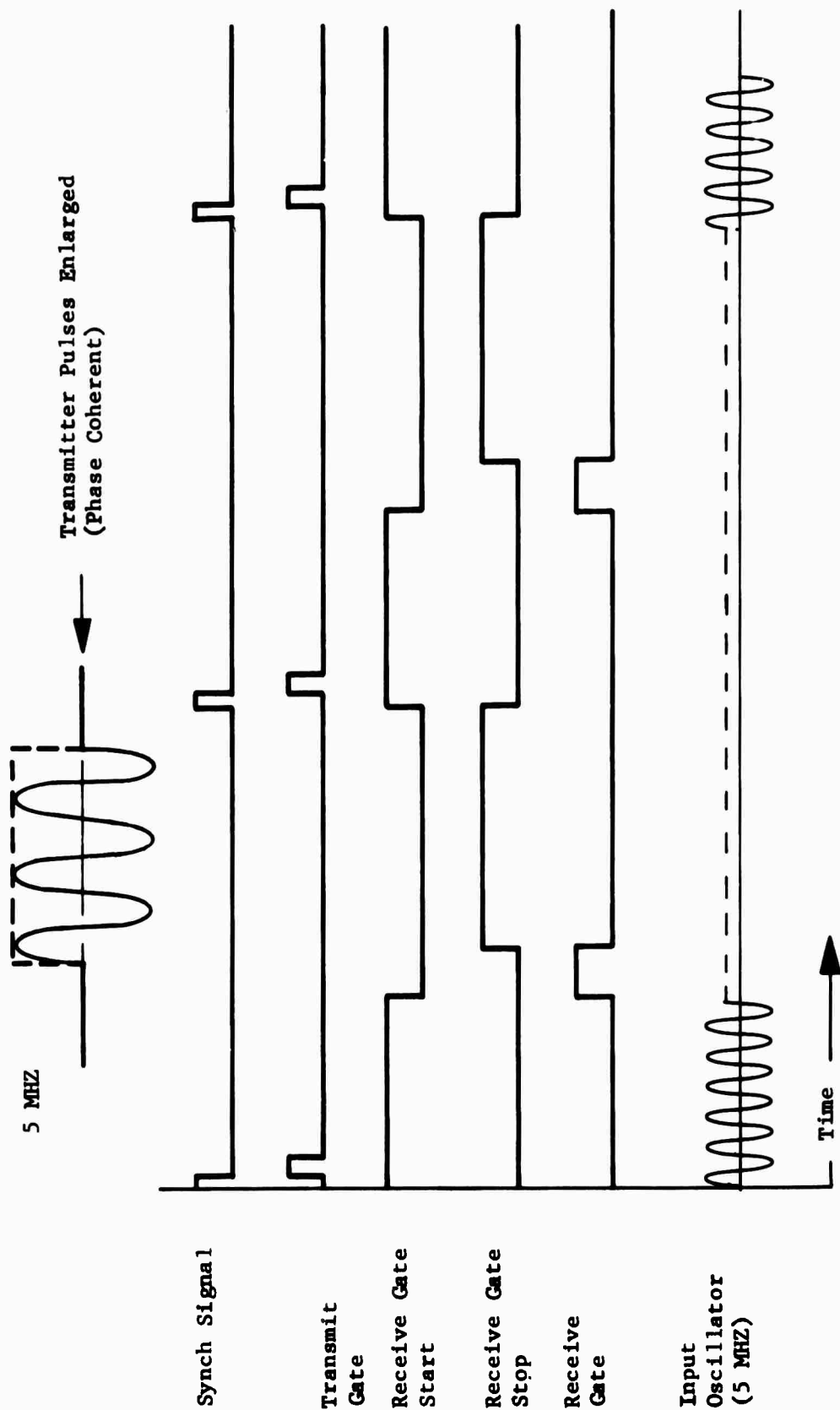


Figure 12. Timing Diagram of New Timer Unit

3. Transmitter

The transmitter is a modification of the previous unit to put out a pulsed carrier which maintains the same phase relationship between the pulse envelope and the carrier for every transmitted pulse. As may be seen in the overall block diagram, Figure 9, this is accomplished by combining the carrier and the phase-locked transmitter gate in a balanced mixer and then amplifying the resultant pulsed rf. The mixer is a Hewlett-Packard Type 10534B double-balanced (ring) modulator used as a pulse amplitude modulator. It operates at 5 milliwatt (0.5 V rms into 50 ohms) rf input and produces a clean pulse output of approximately the same power level. A transistor amplifier was added to increase the level of the pulsed signal to drive the vacuum-tube power amplifier used in the previous system.

4. Receiver-Light Modulator

The requirements for the receiver portion of the system are that it multiply the 5 MHz reference sine wave by the pulsed sine wave received signal and integrate the product over a preselected range-gated interval. The value of the integrated product must be sampled at the end of the integration time and used to control the intensity of the light-emitting diode which exposes the film to construct the hologram. The receiver-light modulator consists of three blocks in Figure 9, the receiving transducer preamp, the receiver itself, and the light modulator.

The receiving transducer preamp is the same one used in the early phases of this program, and its schematic diagram is shown in Figure 13. It is mounted with the point-source receiving transducer in a plastic shell on the scanning carriage. Its gain is controlled by varying the 0 to 12 V dc supply voltage.

The receiver proper uses a Hewlett-Packard type 10534 balanced mixer to multiply the 5 MHz reference sine wave by the 5 MHz received signal (pulsed) scattered from the specimen. The mixer operates at 1-5 milliwatt level with a conversion loss of 6 db.

The components of the mixer output which are of use in generating the hologram are the dc term and frequency components up to approximately 1 MHz necessary to reproduce a 1 microsecond pulse. These are filtered from the mixer output by a low-pass filter with a two-pole attenuation characteristic. For ease in implementation, an active filter built with an integrated circuit chip is used. The attenuation characteristic of the filter is approximately 12 db at twice the cutoff frequency with an ultimate attenuation of 40 db per decade. Since the filter only has a gain of unity, it is followed by an amplifier before integration.

A schematic diagram of the receiver mixer-amplifier is shown in Figure 14. A Melcor type 1672 integrated circuit amplifier is used to provide the 1 milliwatt of signal power to the mixer, while a Fairchild type μ A 702

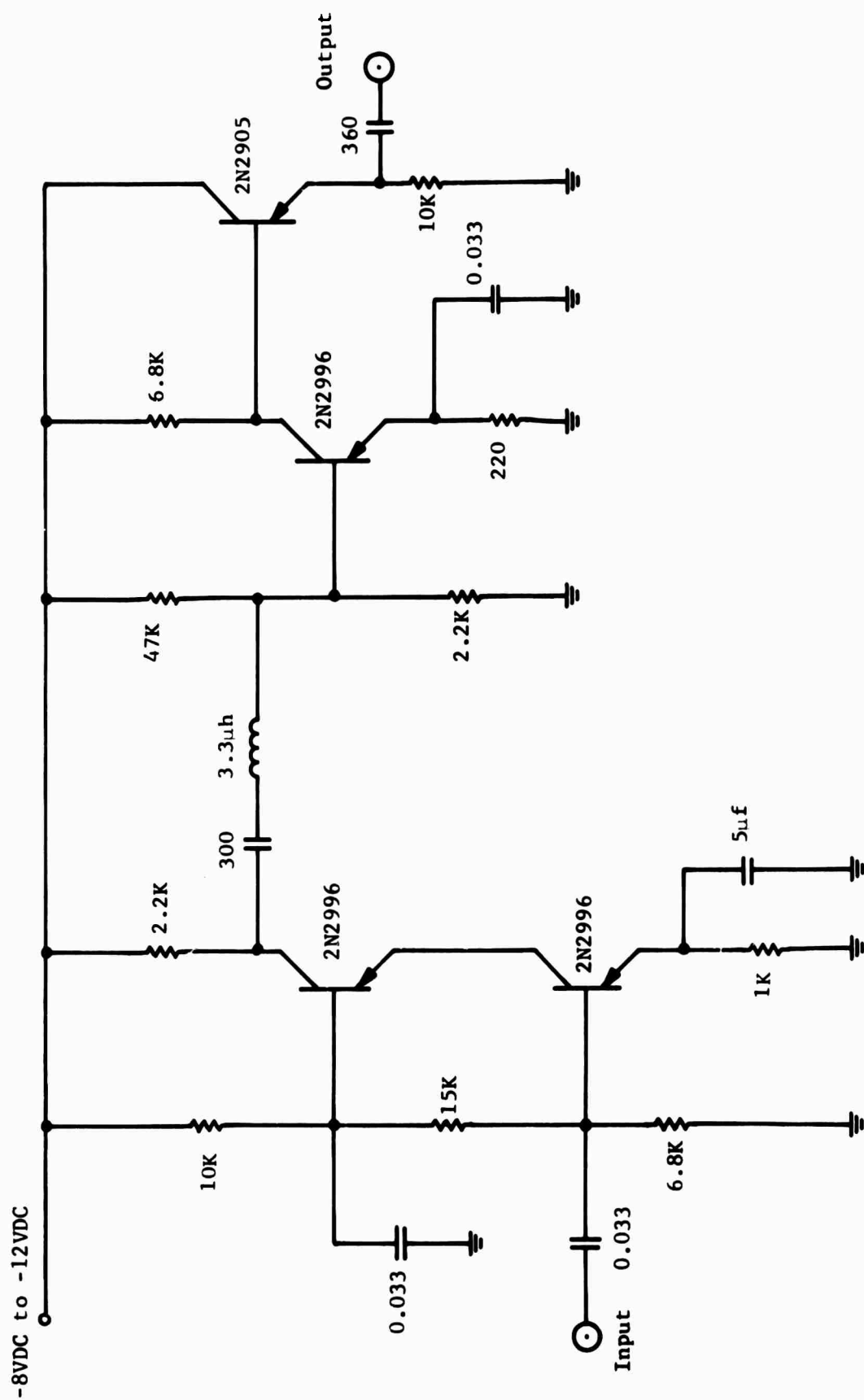


Figure 13. Schematic Diagram-Receiver Preamplifier Unit

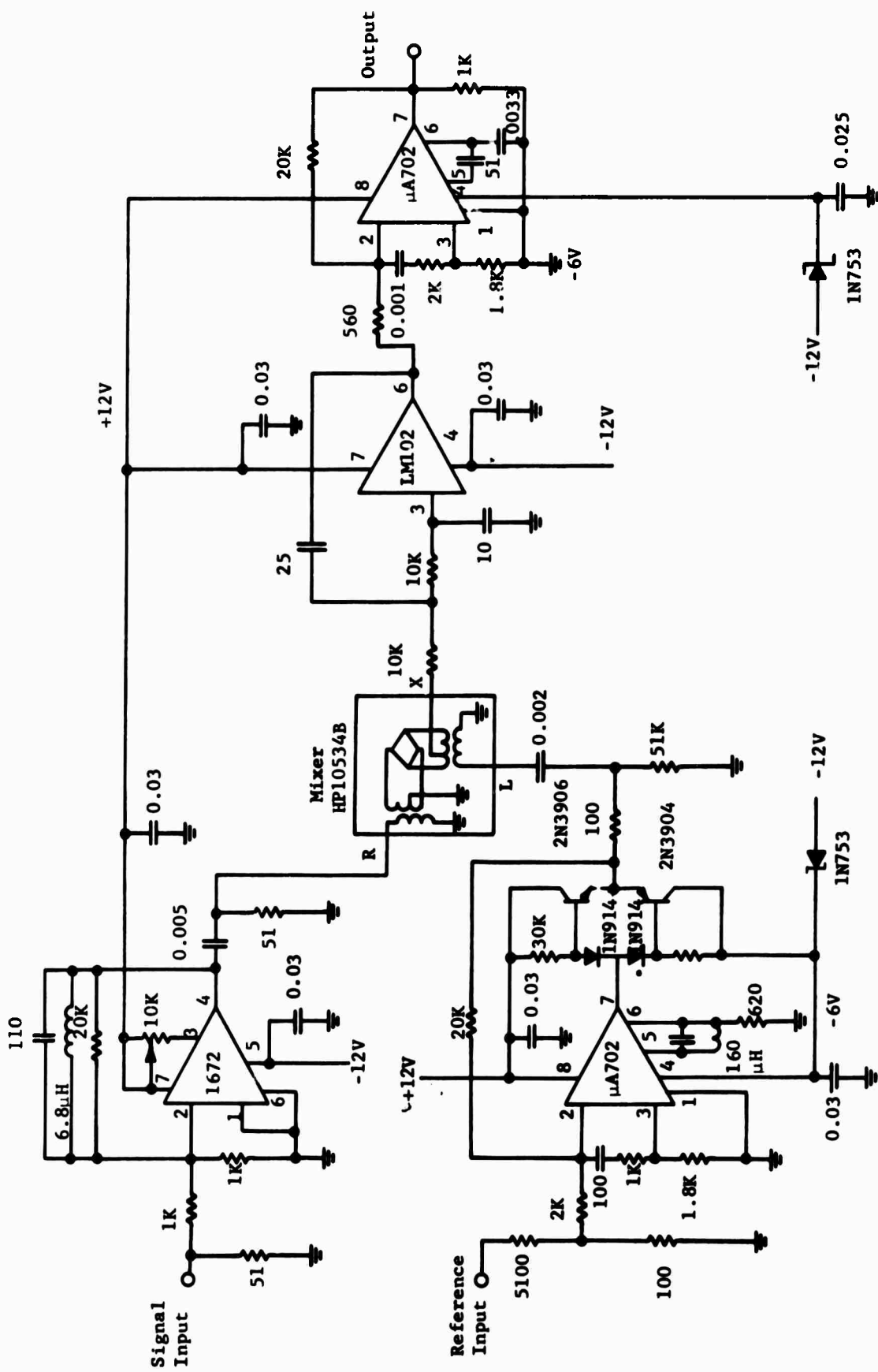


Figure 14 . Schematic Diagram - Receiver Mixer/Amplifier

integrated circuit amplifier plus a pair of transistors is used to provide approximately 5 milliwatt of 5 mHz reference signal. The active filter uses a National Semiconductor LM 102 linear integrated circuit, and the output amplifier is another $\mu A702$. The signal gain from input to output is approximately 30 db, typically a 10 milliwatt signal from the preamp providing about 0.30 volts output for the integrator.

The integrator is the heart of the holographic camera receiver and considerable care had to be spent in its design and construction. The requirements for this circuit are that it integrate the product of the received signal and the 5 mHz reference signal over a preselected range-gate interval, and then "hold" the integrated value until it can be "sampled" by the light pulser which follows. Upon completion of the sampling, the integrating capacitor must be discharged prior to the initiation of the next cycle. The circuit must be capable of recycling at repetition rates of 10 to 10,000 Hz, and for combinatory values of transmitted pulse width, receiver-gate delay, and receive-gate width.

The timing relationship for the functions of the gated-integrator is illustrated in the timing diagram of Figure 15 along with the corresponding timing of the overall system. As shown on the diagram, integration to either positive or negative values of voltages ($+V_1$ or $-V_2$) takes place during the duration of each receive gate, and the integrated value held for sampling. The sampling hold time extends until the next transmit pulse, at which time the integrator capacitor is discharged back to zero volts. Note that the hold circuit must maintain the integrator capacitor at zero volts from the time it is discharged up to the next integrate interval, as well as holding the integrated value for sampling immediately following the integration time.

The schematic diagram of the gated-integrator is shown in Figure 16. The integrator itself is a Fairchild linear integrated circuit, $\mu A702$, but it operates in conjunction with two insulated-gate field-effect transistors (IGFET) as switches to provide the "hold" and "discharge" functions. The sequence of operations may be followed with the schematic, Figure 16, and the timing diagram, Figure 15.

Integration takes place during the receive-gate interval. During this time, switch S1 (IGFET) is closed so that capacitor C1 may be charged through resistor R1. Switch S2 (IGFET) across the integrating capacitor is open during this time interval. Immediately upon completion of the integrate interval, S1 is opened to "hold" the charge on C1 for sampling by the light modulator. Switch two (S2) remains open during the hold interval, but closes during the transmitter gate interval to discharge capacitor C1 and terminate the cycle. Note that the open switch S1 which accomplishes the "hold" action is still open during the discharge time so that it also holds the zero voltage on capacitor C1 from the end of the transmit gate to the start of the receive gate. This ensures a completely discharged capacitor prior to the start of each integrator interval.

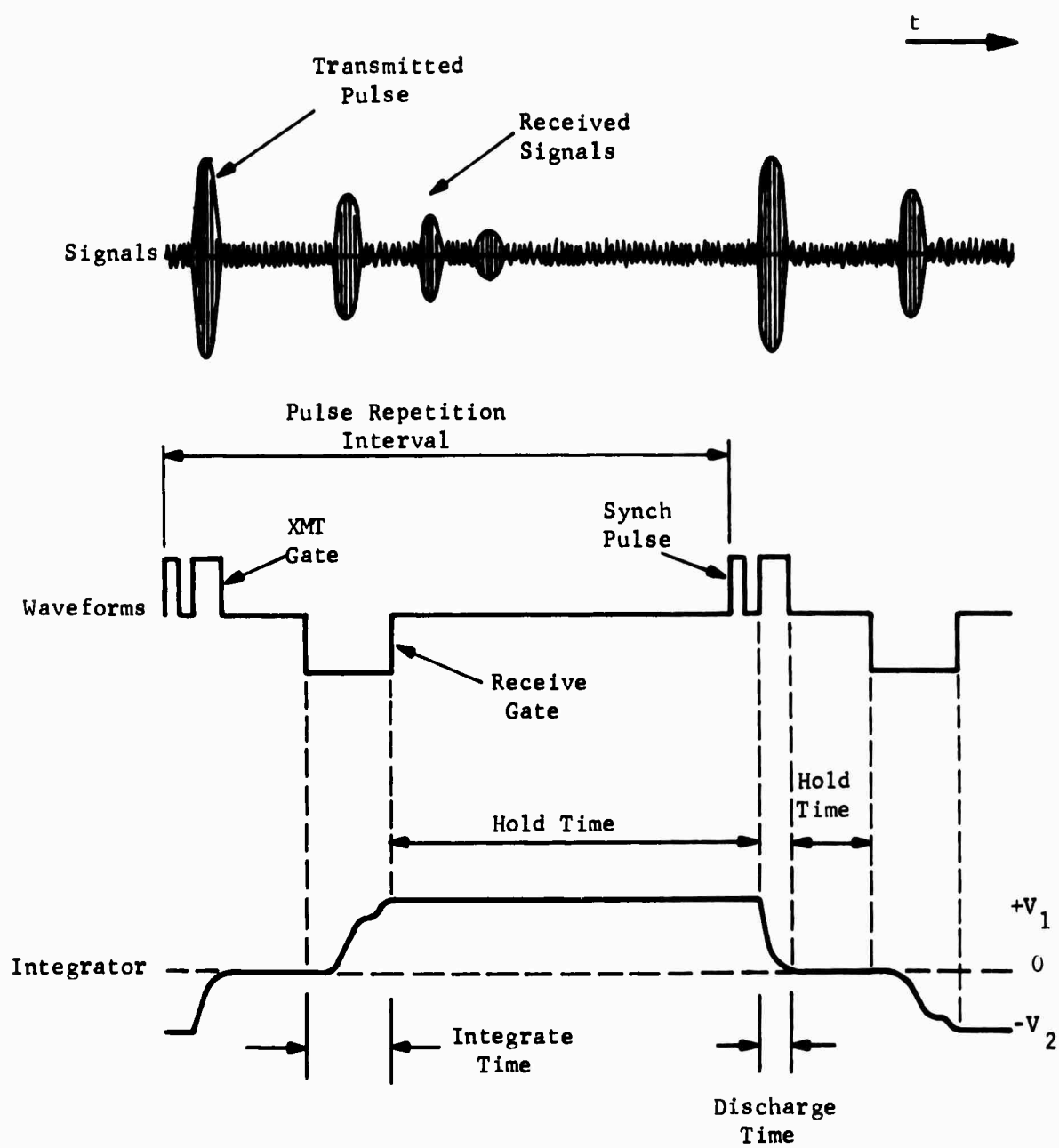


Figure 15 . Timing Diagram - Gated Integrator

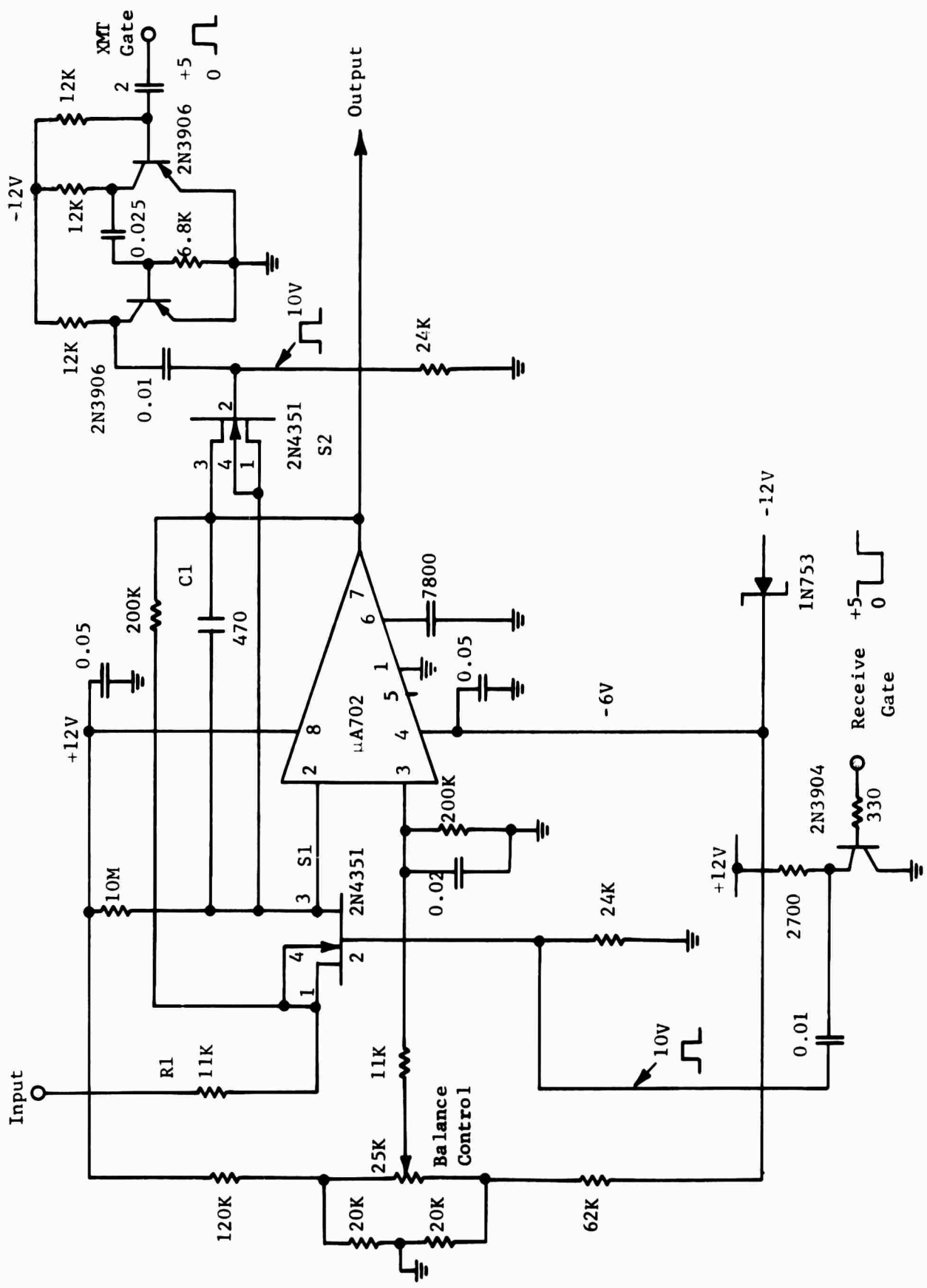


Figure 16 . Schematic Diagram - Gated Integrator

The 2N3904 and 2N3906 transistors shown in the schematic diagram of the integrator, Figure 16, provide the proper amplitude and polarity of the transmit and receive gates for the 2N4351 IGFET switches.

The design of the new light modulator was based on values of average light intensity derived from the earlier tests. In those tests the light-emitting diode was operated at 5 volts potential with an on-time of approximately 100 microseconds and an off-time of 900 microseconds when using a pulse repetition rate of 1000 pps. The resulting brightness permitted lens openings of f:5.6 to f:8 to be employed with high-definition, low-speed film.

In the new modulator the average value of light on-time was made adjustable from approximately 50 microseconds to 500 microseconds, although a nominal value of 250 microseconds is expected to be used for most of the recording.

The timing sequence of the light modulator with relation to the other important system waveforms is shown in the timing diagram of Figure 17. In this diagram it may be seen that the light is turned on at the end of the receiver gate (line 5 of Figure 17) and turned off before the start of the next transmission cycle. The turn-off time is made proportional to the integrator output by comparison of the integrator output with a time ramp, as indicated at point A on lines 3 and 4 of the timing diagram. The modulator is calibrated by setting the integrator output to zero volts and biasing the time ramp to produce a 250 microsecond long output pulse for the light, as indicated at point B on lines 3 and 4. As the integrator output voltage swings positive and negative around zero, the light is modulated about the 250 microsecond nominal value, as shown in the bottom line of Figure 17.

The schematic diagram of the light modulator is shown in Figure 18. Integrated circuit chips are used for the comparator (LM710), the ramp generator (LM201), and the flip-flop (SN7474N). A 3N155A field-effect transistor (FET) is used to unclamp the ramp generator during each cycle. During operation, the light diode is turned on by the trailing edge of the receive gate and turned off when the ramp voltage equals the integrator output voltage at the comparator. R1 is a calibration control which permits the light duration to be set as its nominal value (250 μ seconds) when the input to the modulator is zero volts.

Figures 19 through 23 are photographs of typical signal waveforms existing at key points within the new ultrasonic holographic camera. Different time scales are used in the photographs to best illustrate the significant features. The transmitted pulse is at the extreme left-hand side of the photographs. Two traces appear on each photo to enable signal waveforms at two different points in the system to be compared simultaneously.

The lower trace in Figure 19 is an input signal to the transmitter. It is a 5 microsecond pulse of a 5 Mhz carrier with the pulse envelope phase-locked to the carrier to maintain the same phase relationship for every pulse. The upper trace shows the output of the transmitter when excited by the lower waveform and driving a quartz transducer submerged in water. The output is the voltage coupled to the transducer.

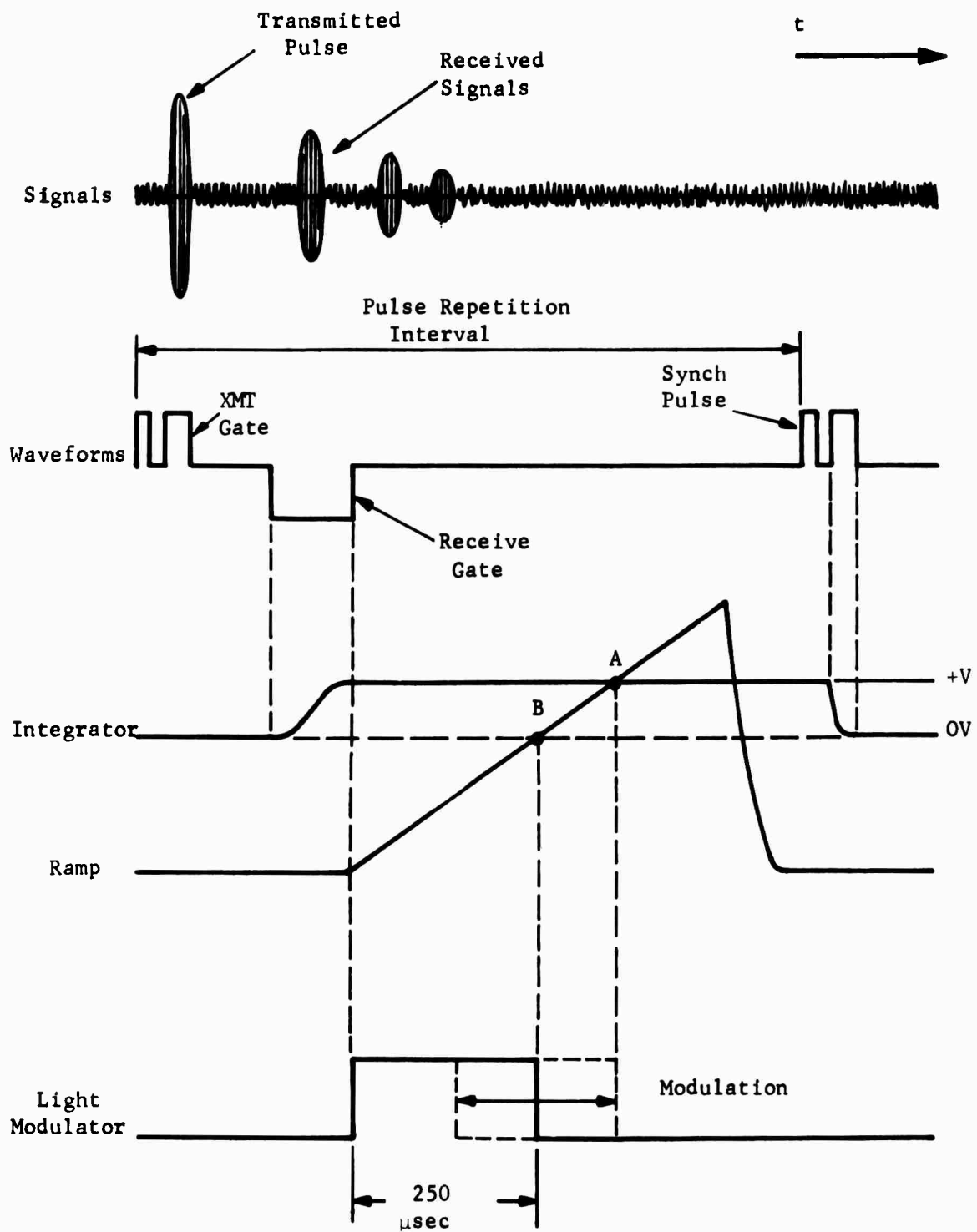
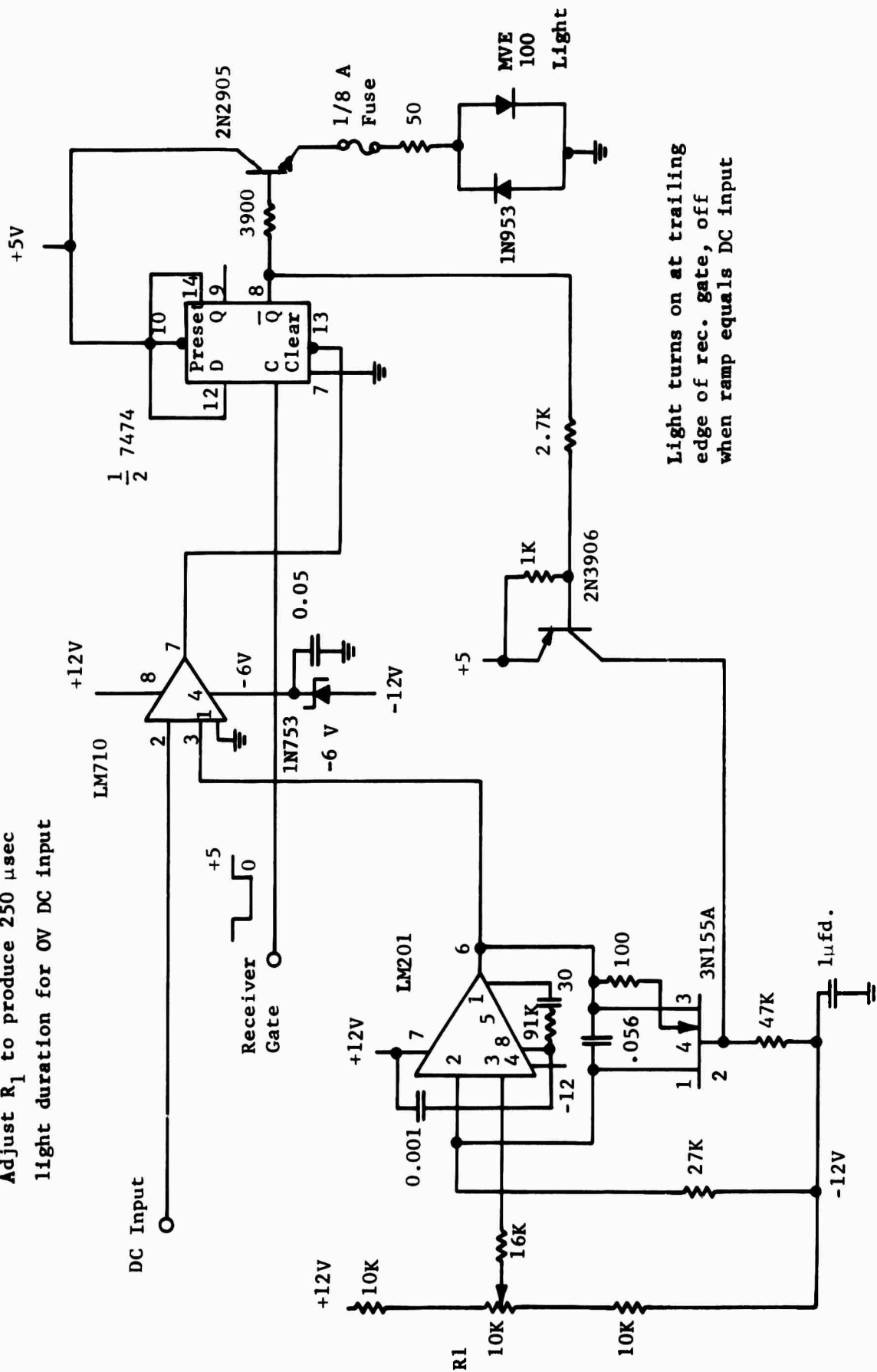


Figure 17 . Timing Diagram - Light Modulator

Adjust R_1 to produce 250 μsec
light duration for 0V DC input



Light turns on at trailing
edge of rec. gate, off
when ramp equals DC input

Figure 18 . Schematic Diagram-Light Modulator

The upper trace in Figure 20 shows the received signal at the input to the receiver mixer (multiplier). The received signal is the signal return from a 1.6 millimeter diameter wire mounted under water approximately 20 cm. in front of the transmitting transducer. The point-source receiving antenna is in the water approximately 10 cm. above the wire. The transmitted pulse length is 10 microseconds. The waveform of the received signal at the mixer is identical except in amplitude to the waveform of the signal out of the receiving transducer. The lower trace shows the output from the receiver after multiplication with the 5 Mhz reference signal in the mixer, filtering through the low-pass filter and amplification. Since this output waveform is the product of the received signal times the reference, it is a bipolar signal whose amplitude and polarity depend on the phase relationship between the two inputs. As the receiving antenna carriage is moved, the signal in the lower trace of Figure 20 changes amplitude and polarity in response to the phase and amplitude of the received signal.

Figure 21 contains photographs of the receiver mixer output before (upper trace) and after (lower trace) the low-pass filter. Since the multiplication of the received signal times the reference signal produces a strong double frequency component of 10 Mhz as well as the dc output (pulse) containing the phase and amplitude information, a low-pass filter is used to remove the 10 Mhz component while still perserving the fidelity of the pulse. The 10 Mhz frequency component may be observed on top of the pulse in the upper trace photograph.

In Figure 22 the signal at the input to the mixer is shown on the upper trace and compared with the output of the integrator on the lower trace. The location and duration of the receive gate are indicated by the small pips on both traces on either side of the received or integrated signals. The width of this gate defines the extent of the integration interval. Immediately following the integration interval on the lower trace is the "hold" interval, during which time the amplitude of the integrated signal is maintained constant for subsequent sampling. Not shown on the integrator outpt is the "clamping" period when the integrator capacitor is discharged back to zero volts. This occurs during the time of the transmitted pulse which is off to the left on the photograph. It should be noted that the integrator hold signal may be positive or negative (above or below the zero axis) according to the polarity of the input signal.

In Figure 23 the pulse waveform applied to the recording light is shown on the upper trace and compared with the integrator output on the lower trace. It can be seen that the pulse for the recording light commences at the end of the receive gate (marked by the small pips) and extends for a duration of approximately 250 microseconds. The length of the pulse is usually set to 250 microseconds when the output of the integrator is zero volts, and is more or less than the 250 microseconds nominal value as the integrator output varies about the zero voltage value.

5. Mechanical Scanner

As mentioned earlier, it is essential that the receiving transducer be scanned in a plane which is flat to within a small fraction of the acoustic wavelength. The present ultrasonic holographic camera operates at 5 megahertz

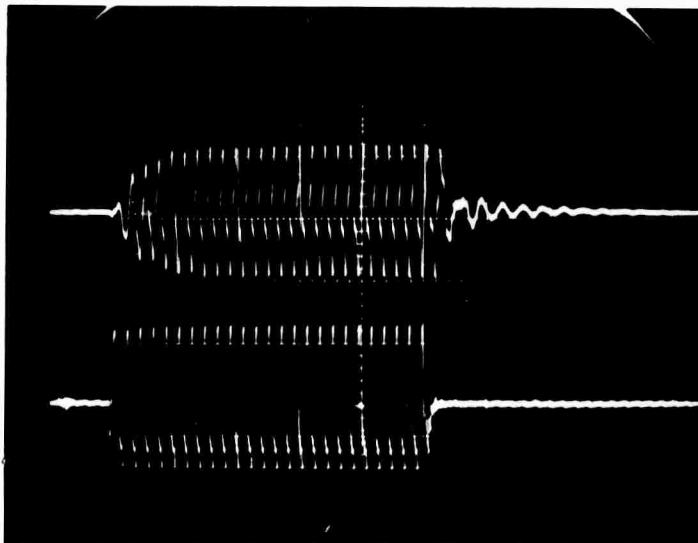


Figure 19. Waveform Photographs:

Upper - Transmitted Pulse to Transducer (5- μ sec).
Lower - Input Pulse to Transmitter (5 μ sec).

Time Scale 1- μ sec/cm

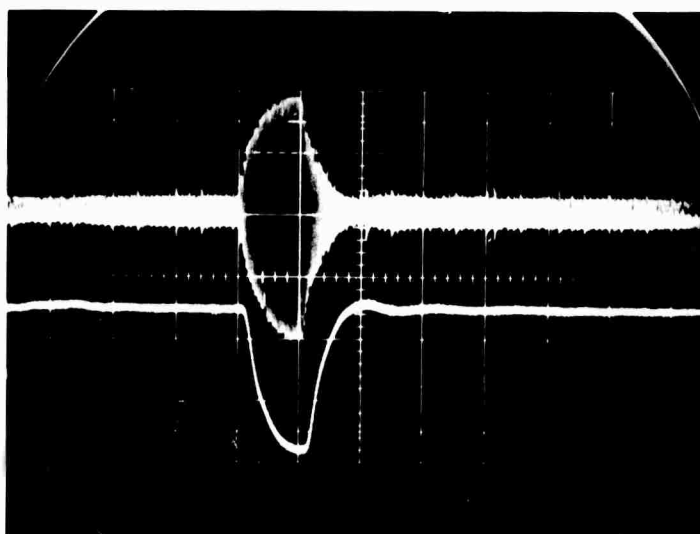


Figure 20. Waveform Photographs:

Upper - Signal From Wire at Input to Receiver Mixer
Lower - Output of Receiver After Multiplication With
Reference and Low-Pass Filtering

Time Scale 10 μ sec/cm

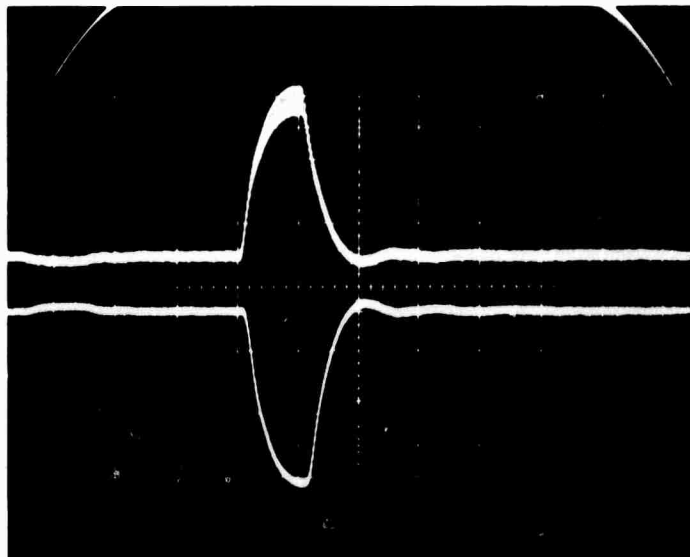


Figure 21. Waveform Photographs:
Upper - Received Signal at Input to Low-Pass
Filter
Lower - Output of Receiver After Filtering
Time Scale 10 μ sec/cm.

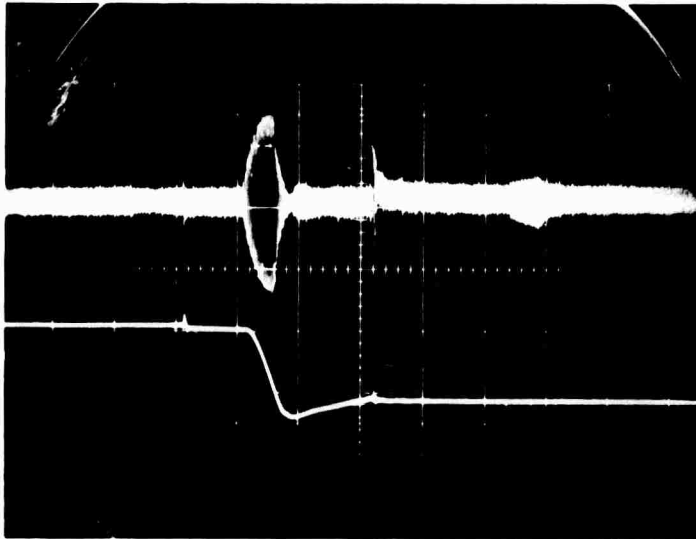


Figure 22. Waveform Photographs:
Upper - Received Signal Out of Preamp.
Lower - Output of Gated Integrator

Time Scale - $20\mu\text{sec}/\text{cm}$

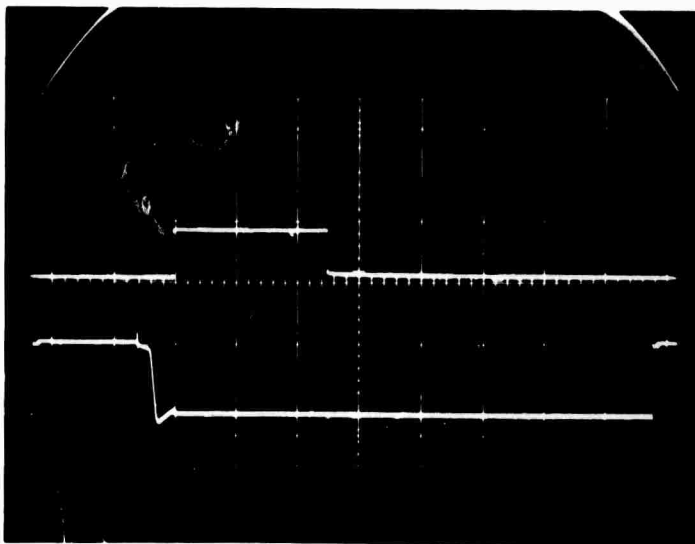


Figure 23. Waveform Photographs:
Upper - Modulated Pulse to Recording Light.
Lower - Output of Gated Integrator.

Time Scale - $100\mu\text{sec}/\text{cm}$

with a water medium coupling both transmitting and receiving transducers to the specimen. Therefore, the acoustic wavelength is 300 microns (approximately 12 one-thousandths of an inch). This implies that the plane in which the receiving transducer is scanned should be flat to within approximately 1/1000 of an inch.

In order to measure the characteristics of the X-Y scanner, the setup shown in Figure 24 was utilized. A Brown and Sharpe microinch gauge was connected to the X-Y scanning track in place of the receiving transducer. A granite surface plate was mounted in close proximity to the track so that its surface could be sensed. The granite surface plate was in turn supported by a jig plate and three kinematically-mounted rods. The X-Y scanner was then activated and the output of the Brown and Sharpe gauge recorded on an oscilloscope as a function of position, as well as a function of three different scan velocities (3 seconds per scan, 6 seconds per scan, and 12 seconds per scan). Both single scans and composite (repeated) scans were recorded. The total travel per scan was seven inches.

It was found that the results were essentially independent of speed over the speed range mentioned above. A single scan is shown in Figure 25 (taken at 12 seconds per scan), and a composite scan (taken at 3 seconds per scan) is shown in Figure 26. The low frequency periodic fluctuation in the distance between the surface plate and the pick-up head was found to be due to a slightly elliptical riding wheel on the transducer carriage. Even with the mechanical variations shown in Figures 25 and 26, the departure of the traverse from flatness is within $\pm 1/20$ of an acoustic wavelength. This met the requirements given above and no action was required to improve the "flatness" of the X-Y scan mechanism.

Additional measurements were made of the opto-mechanical performance of the system by traversing the scanner mechanism while simultaneously pulsing the light-emitting diode from a constant repetition frequency pulse generator. The purpose of this experiment was to track down what appeared to be pulse-position modulation which occurred in holograms made on the previous contract. Figure 27 shows the photographic recording which resulted when the scanner traversed at 1 inch per second and the light-emitting diode was pulsed at 125 pulses per second with a pulse width of 2 milliseconds. Several adjacent scan lines are displayed. It is evident that orthogonal to the scan direction there is a "grating-like" positional modulation which occurs at a relatively high spatial frequency. This frequency was found to be directly related to the pitch of the worm gear which drives the scanner. Using a Strobotac it was found that the servo motor driving the scanner ran at a rate which was proportional to its torque loading. Since the torque loading depended upon the position of the worm gear, the worm gear was being driven at a nonuniform angular velocity.

In order to correct this situation and remove the striations from the holograms, a new motor drive system has been designed and is being built. The new drive system uses a constant-speed synchronous motor for the fast-scan direction, and a dc stepping motor for the slow-scan drive. Also, the nut engaging the fast-speed worm is being modified to provide an antibacklash carriage so that the fast scan may be used in both directions without objectionable hysteresis effects. At the present time, the recording light is blanked out during one direction of scan to eliminate any hysteresis effects.

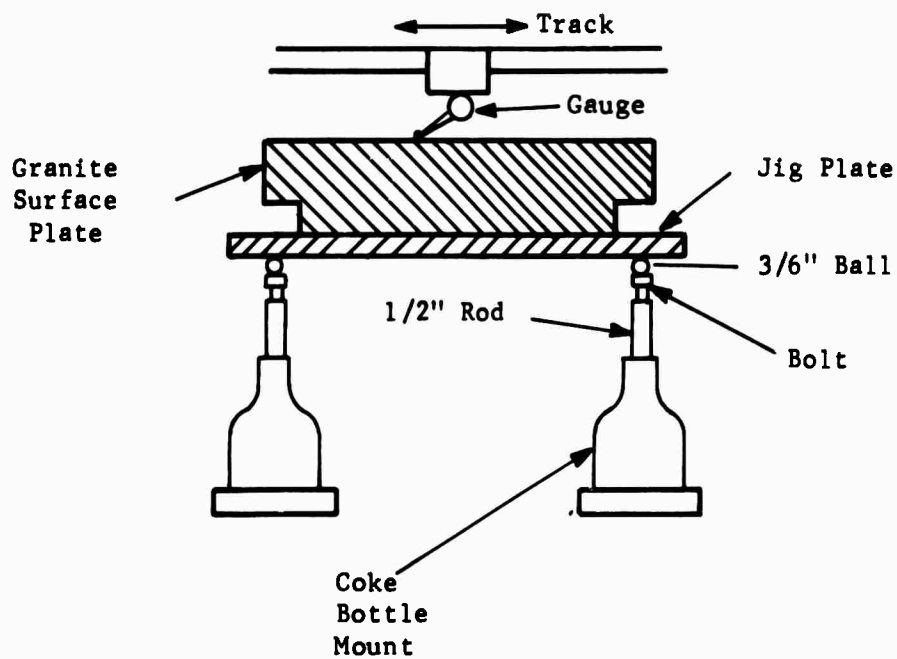


Figure 24 Experimental Set-up for Measuring Flatness of the X-Y Scanning Plane

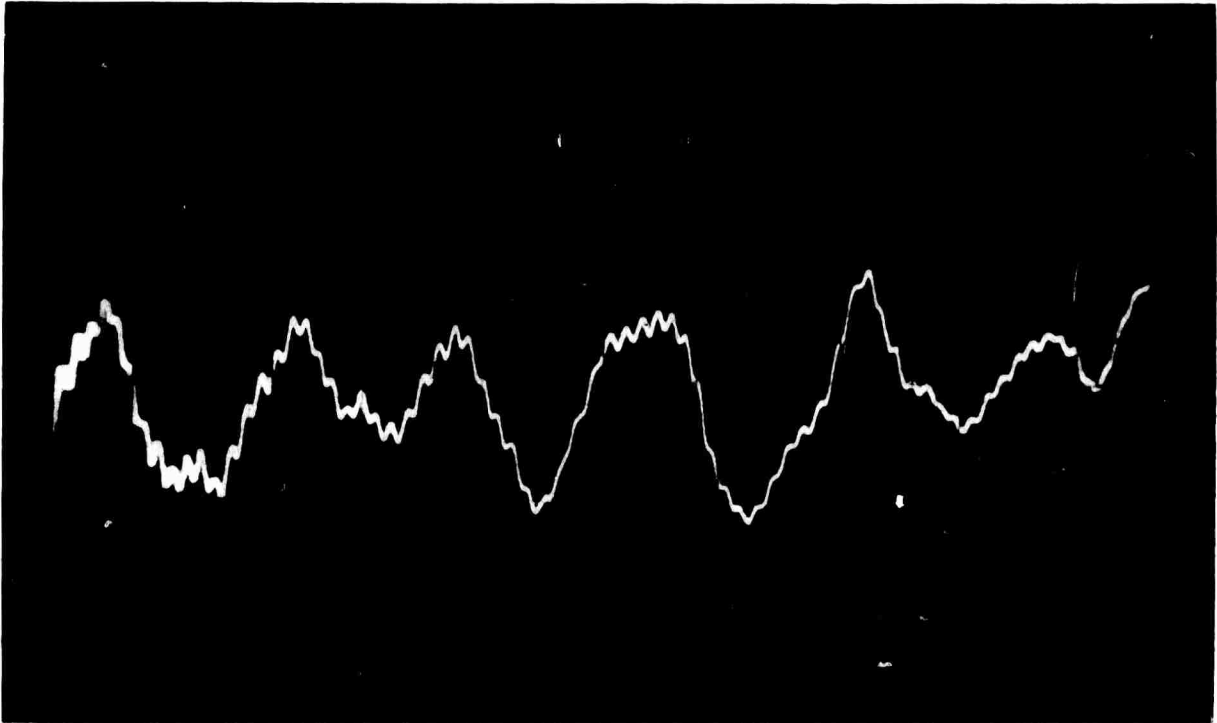


Figure 25. Single Line Profile Across the Scanning Plane (5 μ Peak-to-Peak)

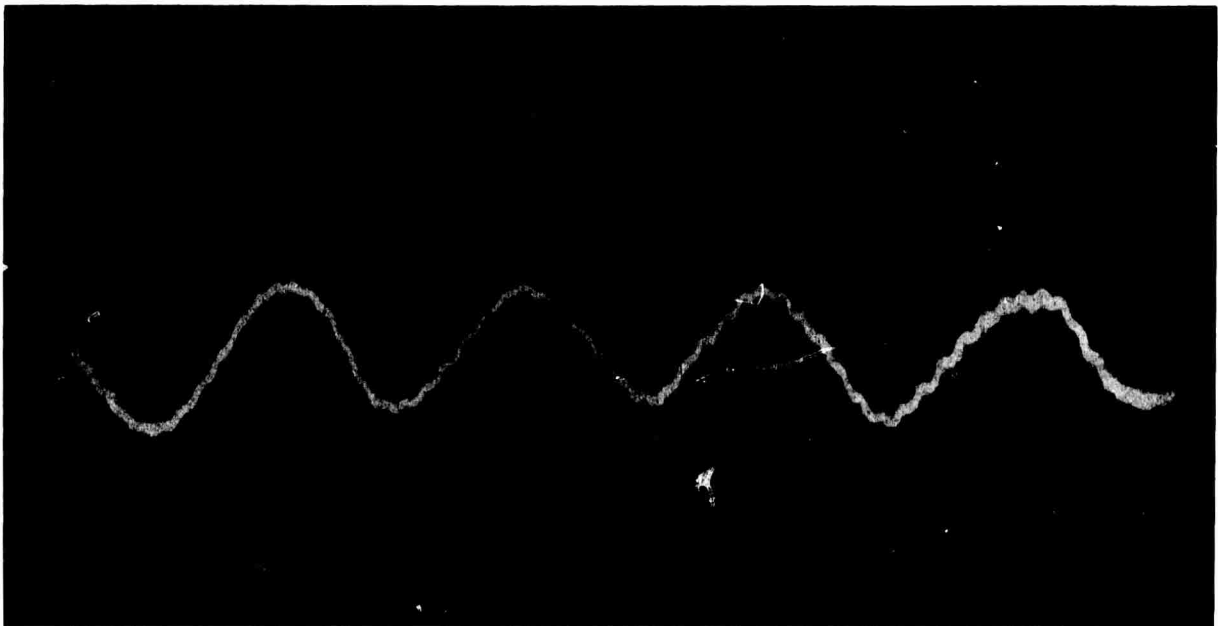


Figure 26. Composite Profile Across the X-Y Scanning Plane (5 μ Peak-to-Peak)

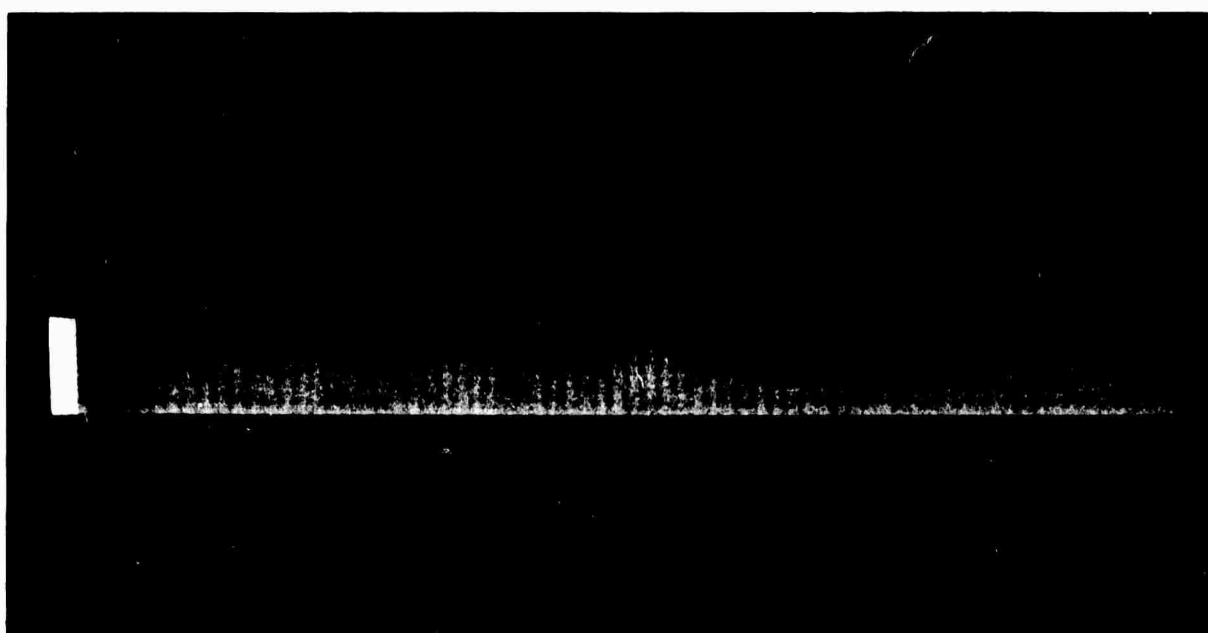


Figure 27. "Grating-Effect" in Artificial Acoustic Hologram due to Velocity Modulation in the X-Y Scanning Plane

A block diagram of the new drive system is illustrated in Figure 28. As shown in the diagram, the fast-scan synchronous motor runs the carriage back and forth under control of microswitches and reversing relays. The slow-scan stepping motor is driven by an electronic pulse generator enabling any number of fine steps to be counted during the turnaround time of the fast-scan drive. This will enable the spacing of consecutive scan lines to be adjusted for the best holograms in the least possible scan time. The electronic pulse generator has been provided with a rapid slew mode for the step-motor drive to enable the carriage to be moved rapidly during set-up and test.

C. EXPERIMENTAL RESULTS

As has been pointed out in this report, a considerable amount of effort has been spent in modifying the ultrasonic holographic camera so that it could have the flexibility of operation required to produce holograms easily and reliably for many combinations of system and subsystem operating parameters. The parameters available for such systematic change encompass all aspects of the recording and imaging process, and include the characteristics of the transmitted signal, the receiver gating, and the receiver processing; the geometry of the transmitting and receiving paths; the nature of the specimen; the exposure and the processing of the film; and the technique of reconstructing the image. The effect of variations in these system parameters on the quality of the ultrasonic images produced has not yet been determined experimentally, because of the practical difficulties involved in systematically making the changes required to do this evaluation. Now that the modifications have been made to obtain the flexibility required, routine investigation of the holographic imaging technique for non-destructive testing can proceed.

The first results obtained from the revised system are the signals received from the scattering of a small hole in an aluminum block, shown in Figures 29(a) and (b). In Figure 29 (a) a 10-microsecond transmitting pulse was used to ensonify the inside of the block, while in Figure 29 (b) a 2-microsecond transmitting pulse was used. The receiving transducer was located in water approximately 10 cm above the hole, the hole being parallel to the scanning plane. The received signal, shown in both photographs is the bipolar pulse produced by the multiplication and low-pass filtering process in the receiver, and the amplitude and polarity are sensitive to the location of the receiving transducer, as expected.

The spectrum of signals produced by the 10-microsecond pulse in Figure 29 (a) is typical of the ones obtained with the earlier system which used pulses of 10 microseconds and longer. The primary signal produced by the hole is the large negative pulse occurring approximately 10 microseconds after receipt of the first return from the transmitting transducer itself on one face of the block. The system noise level is shown by the width of the oscilloscope trace at the start of the sweep on the extreme left-hand side.

Figure 29 (b) shows the signals returned from the aluminum block, when the 2 microsecond pulse was used, all other conditions remaining the same as those for Figure 29 (a). Again, the return from the hole is the large negative

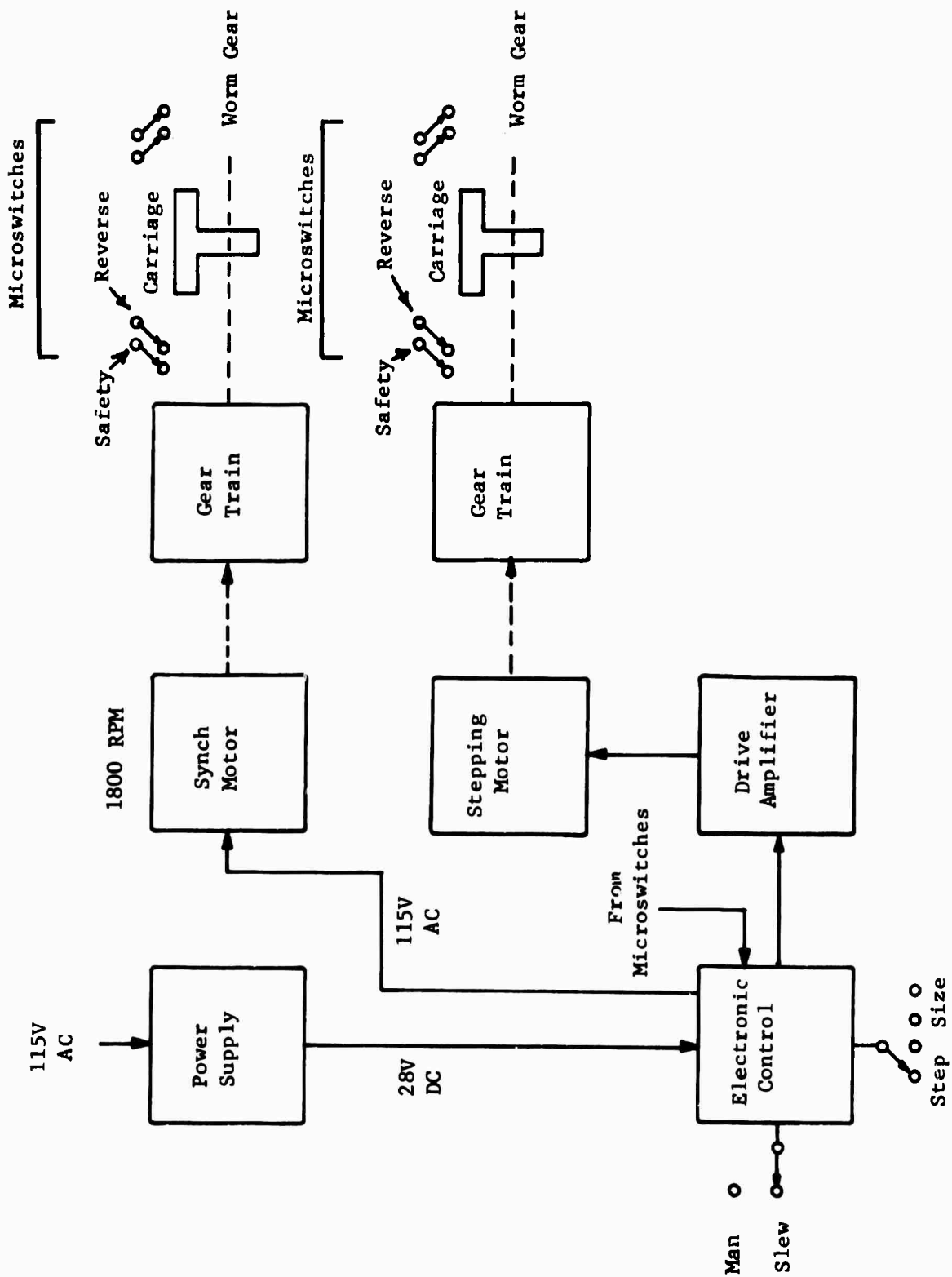


Figure 28. Block Diagram - Mechanical Scanner

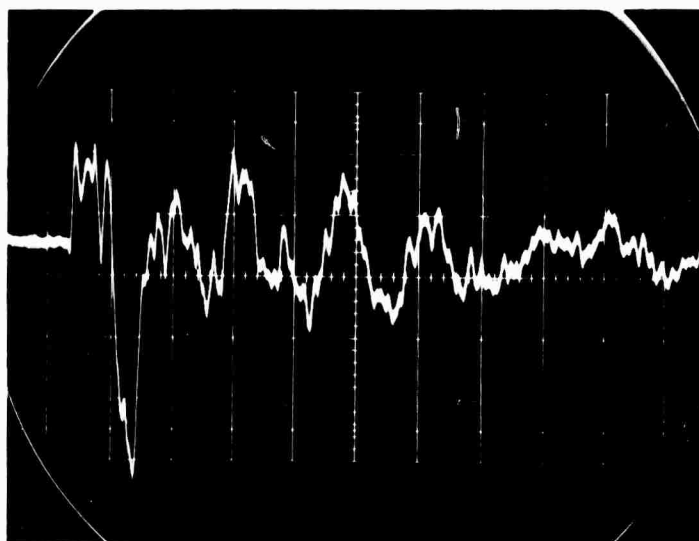


Figure 29(a) Processed Signal from Hole in Block.
Revised System (10- μ sec transmitted Pulse)

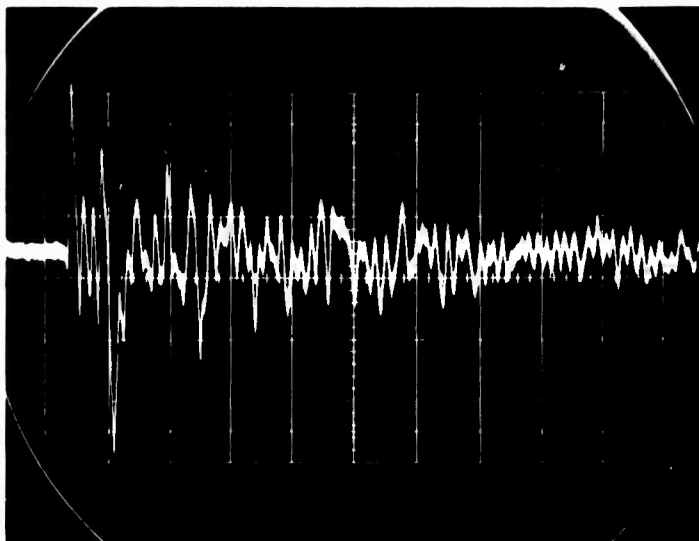


Figure 29(b) Processed Signal from Hole in Block.
Revised System (2- μ sec transmitted Pulse)

spike occurring approximately 10 microseconds after the initial return, and its polarity and amplitude are also sensitive to the receiving transducer location. The characteristics of the remaining echoes, however, are not exactly what had been expected from the previous work done with the 10 microsecond and longer pulses, and from the results of Figure 29 (a).

In Figure 29 (a), for example, it appears that four of five major reflections occur, as would be expected from the many multiple paths within the specimen, and they are separated by time intervals of 20 microseconds, or more. When the two microsecond pulse is used, however, many additional signals are produced between the supposedly major returns, and the expected sharp delineation of the major returns does not occur. Further tests are being made to determine the cause of this phenomenon.

The first hologram produced by the revised system is illustrated in Figure 30 at approximately one-half real size. A simple target consisting of a single aluminum wire approximately 1.6 mm in diameter was used for this initial test specimen, so that the results of the holographic imaging could be easily compared with those obtained with the earlier system. For this test a 5-cm diameter quartz transducer with a collimated beam was used to ensonify the specimen perpendicular to the axis of the wire. The transducer was at the same level as the wire, and approximately 20 cm away. The receiving transducer scanned an area of 30 cm x 10 cm approximately 10 cm above the wire.

Because of the large diameter of the transmitting transducer in acoustic wavelengths, its beam pattern was quite sharp, and the near field (Fresnel region) of its radiation in water included the area scanned by the receiving transducer. It is believed that the curved fringes at the ends of the wire, as well as those perpendicular to the axis of the wire along its length, are the mirror image of the near-field pattern of direct radiation from the transmitting transducer.

The image constructed from the hologram of Figure 30 is illustrated in Figure 31 at approximately full size. The image focuses sharply in the optical set-up at the dimension corresponding to its depth below the holographic plane, and is similar to those produced by the previous system.



Figure 30. Hologram of 1.6 MM Diameter Aluminum Wire.
Revised System (10-usec Transmitted Pulse)
1 cm Scale in Hologram Plane

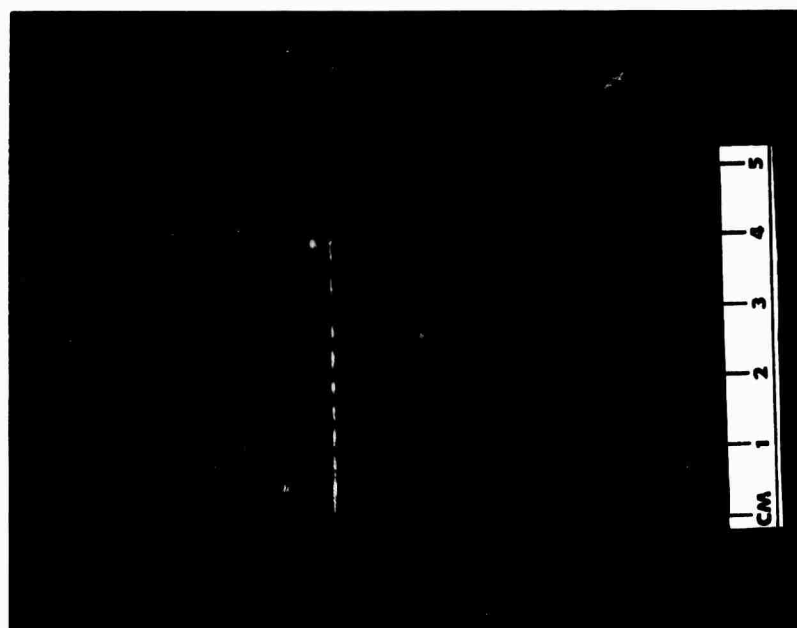


Figure 31. Reconstructed Image of 1.6 MM Diameter Aluminum
Wire, Revised System

SECTION III

ULTRASONIC DIFFRACTION MICROSCOPE

The ultrasonic diffraction microscope should provide higher resolution for smaller specimens than the ultrasonic holographic camera.

The following sections present

- a. A simplified theory of the operation of the ultrasonic diffraction microscope, and
- b. a description of our experiments to date.

A. THEORY

The ultrasonic diffraction microscope uses the linear Bragg angle diffraction of light by the ultrasonic field to form an optical "image" or map of the ultrasonic field.⁷⁻¹⁰ Figure 32 illustrates the principle of operation in two dimensions. A point source of light (l) is weakly diffracted by the ultrasonic waves emanating from a point source of sound (s) in a material transparent to both waves, such as water. The ultrasonic field is weak enough so that only a small amount of the light source (l) is diffracted. This makes the interaction linear. Thus, the optical and acoustic fields can be expanded into sums (integrals) of plane waves, and each differential plane-wave component treated alone. Each point source is expanded as a uniform distribution of plane waves propagating in all directions whose relative phases are the same at the center of the point. This is represented by the "rays" starting from the point sources. These rays are actually the propagation vectors of the plane-wave components of the point sources. Wherever rays intersect, the corresponding plane waves have similar phases. Where many plane wave components have similar phases, they interfere constructively to produce a bright point image.

Each ultrasonic plane-wave component diffracts a small portion of an optical plane wave only if the two waves are at the Bragg angle. The diffracted wave is also a plane wave propagating at the diffraction Bragg angle. The fraction of the optical plane wave diffracted is proportional to the ultrasonic plane wave component involved. The temporal frequency of the diffracted optical plane waves differs from the incident optical plane waves by the ultrasonic temporal frequency. This frequency shift will be ignored for now. The ultrasonically-diffracted optical field contains one optical plane-wave component for each ultrasonic plane-wave component and, thus, produces an image of the ultrasonic field.

The following analysis of Figure 32 will show that the optical plane-wave components leaving the optical point source (l) and diffracted by the ultrasonic point source(s), appear to have originated from the point (i). The larger

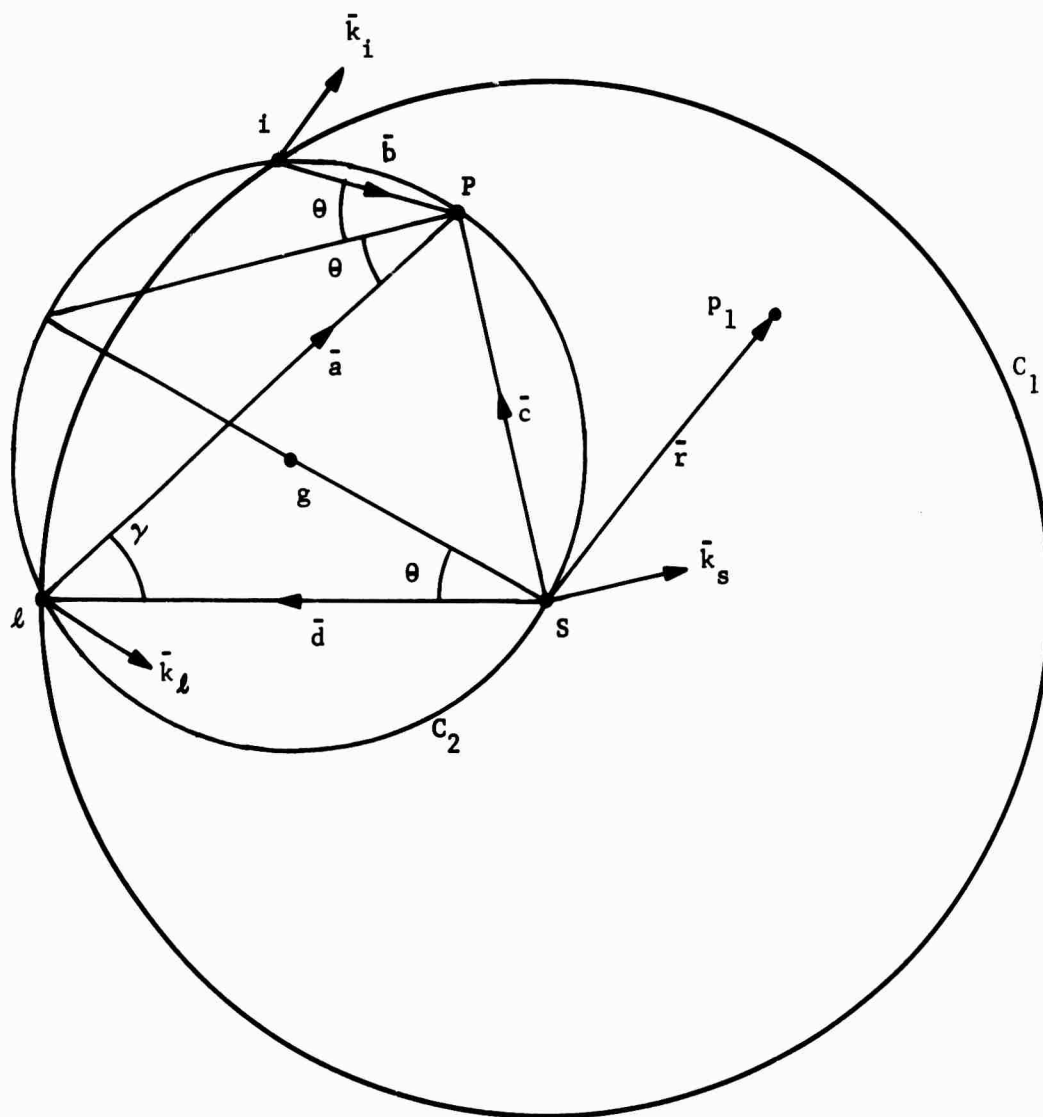


Figure 32. Bragg Angle Imaging Relations

circle (C_1) has a radius (d), where (d) is the distance from (ℓ) to (s), and is centered at the point (s). The small circle (C_2) has a diameter (g) and passes through the points (ℓ) and (s). The following geometric relation results

$$g = \frac{d}{\cos \theta} \quad (3-1)$$

where θ is the Bragg diffraction angle given by

$$|\sin \theta| = \frac{1}{2} \frac{k_s}{k} \quad (3-2)$$

Here, k_s and k are the acoustic and optical wave numbers, respectively.

The following notation will be useful. Bars over variables indicate vectors. The same variable without a bar is the magnitude (always positive) of the vector. The propagation vectors of the optical point-source, acoustic point-source, and optical image are denoted by \bar{k}_ℓ , k_s , and \bar{k}_i respectively. A dot between vectors denotes the dot (scalar) product of the vectors.

The optical image's plane-wave components have a complex amplitude proportional to the product of the optical plane-wave component complex amplitude times the ultrasonic plane-wave component complex amplitude, subject to the condition that these three waves are at the Bragg angle. Thus, the relative phase of a diffracted optical plane-wave component is equal to the phase of the appropriate incident optical plane wave, plus the phase of the appropriate acoustic plane-wave component everywhere. With respect to the vectors shown in Figure 32, this phase relation at an arbitrary point (p_1) is

$$\bar{k}_i \cdot (\bar{r} - \bar{c} + \bar{b}) = \bar{k}_\ell \cdot (\bar{r} - \bar{d}) + k_s \cdot \bar{r} \quad (3-3)$$

It is convenient to let the arbitrary point (p_1) lie on the circle (C_2). That is,

$$\bar{r} = \bar{c} \quad (3-4)$$

and the point (p_1) coincides with the point (p_0). Equations (3-3) and (3-4) yield

$$\bar{k}_i \cdot \bar{b} = \bar{k}_\ell \cdot \bar{a} + k_s \cdot \bar{c} \quad (3-5)$$

Equation (3-5) can only be satisfied if the three interacting plane-wave components satisfy Bragg angle conditions. Because of the construction of circles (C_1) and (C_2), the three interacting plane-wave components of (ℓ) (s) and (i) will satisfy the Bragg angle condition if their respective propagation vectors (\bar{k}_ℓ) (k_s) and (\bar{k}_i) are parallel to the vectors (\bar{a}) (\bar{b}) and (\bar{c}), respectively; that is

$$\bar{k}_\ell = k_\ell \frac{\bar{a}}{a} \quad (3-6a)$$

$$\bar{k}_s = k_s \frac{\bar{c}}{c} \quad (3-6b)$$

$$\bar{k}_i = k_i \frac{\bar{b}}{b} \quad (3-6c)$$

Also,

$$k_i \approx k_l \equiv k. \quad (3-7)$$

The incident optical wave number is approximately equal to the diffractive wave number because the velocity of light is approximately 10^5 times the acoustic velocity. Equations (3-5) and (3-6) yield

$$k b = k a + k_s c. \quad (3-8)$$

From Figure 32 we can write the following geometric relations:

$$\begin{aligned} a &= g |\cos(\theta - \gamma)| \\ b &= g |\cos(\theta + \gamma)| \\ c &= g |\sin(\gamma)| \end{aligned} \quad (3-9)$$

Equation (3-8) is found to be true when Equations (3-2) and (3-9) are substituted into it with appropriate signs depending upon whether (p) lies between (i)(s), (s)(l) or (l)(i). This implies that (i) is the image of (s), which is what we wished to prove.

We have just described the imaging process in two dimensions; we shall now consider the third dimension. There are two cases of special interest:

- (1) The light source (l) is a coherent line-source emitting cylindrical waves, and
- (2) The light source (l) is a coherent point-source emitting spherical waves.

First we will consider the case where (l) is a line-source. In the third dimension the image (i) is actually a slightly curved coherent line perpendicular to the plane of Figure 32. The acoustic point source (s) has been mapped into a line. A suitable set of high quality cylindrical lenses can be used to compress this line image into a point, to form a one-to-one ultrasonic imaging system.

In the second case, (l) is a coherent optical point-source emitting spherical waves. Figure 32 thus has rotational symmetry about the line (d). Therefore, we may rotate Figure 32 about line (d) as an axis to find that the image (i) becomes a circle centered about the line (d). Circle (C₁) has become a sphere, and circle C₂ has become a doughnut without a hole. The optical image of an acoustic point-source is a circle centered on the straight line drawn through the illuminating optical point-source and the acoustic point-source, and lying on the intersection of the sphere (C₁) and the holeless doughnut (C₂). Acoustic points are mapped into a unique family of circles. It is possible to compress these circles back into point images by optical holographic techniques, using an acoustic point-source, or transparent holographic filter.

A second (compression) point-source of sound located at (L) (or preferably at a one-to-one image of (L) with the source (L) blocked out) can be used to compress the ring image (i) back into a point image. The second point-source of sound must satisfy the Bragg relation

$$\sin\theta_2 = \frac{1}{2} \frac{k_{s2}}{k} \quad (3-10a)$$

where

$$\theta_2 = \left(\frac{\pi}{4} - \frac{\theta_1}{2} \right) \quad (3-10b)$$

and

$$\sin\theta_1 = \frac{1}{2} \frac{k_{s1}}{k} \quad (3-10c)$$

Subscripts 1 refer to the illuminating ultrasonic wavelength, and subscripts 2 refer to the second compressing acoustic source.

For the correct intensity compression acoustic source, one-half of the ring energy is compressed to a point image. The image is correctly scaled by the illuminating ultrasonic and light wave numbers at a distance $\left(\frac{k_{s1}}{k}\right) d$ from (L) along \bar{d} . The other half of the energy goes into a new ring that need not be considered at this point. The detailed theory of this process is being analyzed, the following paragraphs indicating the current viewpoints held.

From a practical point of view, the acoustic frequency of the second acoustic source is too high for liquids because the acoustic attenuation is too high. The required frequency is approximately 5 gigahertz for our experiments using water. Such a frequency could be used in solids.

We next ask whether a lower frequency could be used if we magnify the image of (L)? The answer to this question appears to be no, because optics can only magnify planes linearly. Volumes cannot be magnified linearly. Thus, in a magnified image, (i) will not be a spherical wave, although the acoustic source will be. In spite of this, a scaled image using a lower acoustic frequency could probably be made to work. However, there appears to be a simpler way to accomplish this task.

We can replace the compression acoustic point-source by a holographic transparency. The compression acoustic point-source has spherical symmetry, whereas the holographic transparency does not. That is, the optical plane-wave components of (i) see the same index gradient independent of their direction of propagation, because of the spherical symmetry of the compression acoustic source. The holographic transparency does not have this symmetry, and looks different from different directions because of an obliquity factor that states, in effect, that $\sin\theta \approx \theta$ only for small angles. However, if we magnify the plane perpendicular to \bar{d} , the angular extent of the plane-wave components of (i) is reduced. Enough magnification is required so that the optical plane-wave components of the ring images (i) (from the volume to be imaged near (θ)) fall within a small angle of \bar{d} , such that $\sin\theta \approx \theta$ by conventional optical tolerances.

The required holographic transparency should consist of radial zones of half-wavelength phase steps, spaced concentrically at the nulls of the zero-order Bessel function. The outer cycles of the zones should be spaced a distance (Λ_0) apart, referred to the unmagnified space, where

$$\sin \theta_2 = \frac{k_0}{k} \quad (3-11a)$$

$$\text{for } k_0 = \frac{2\pi}{\Lambda_0} \quad (3-11b)$$

determines the scale of the holographic filter.

B. EXPERIMENTS

We chose to do our preliminary experiments with a (spherical) point-source because:

(1) we wanted a diffraction-limited optical system so that we could compare our experimental results to the theory. Also, diffraction-limited spherical lenses of suitable characteristics were more readily available than cylindrical lenses, and

(2) if successful, the point-source system uses spherical optics which are more easily made than large cylindrical optics.

Figure 33 is a schematic diagram of our experiment. Lens (L_1) provides the optical point-source (L). The acoustic point-source(s) is the point image formed by a plane transducer and an acoustic spherical mirror. The Bragg diffraction takes place in water in a tank with two optical windows. Lens (L_2) corrects optical spherical aberration when the light leaves the tank. Lens (L_2) has a center of curvature approximately at the focus of lens (L_1). Lens (L_3) is a relay lens which images the (virtual) image from the tank into lens (L_4). Lens (L_4) is a short focal length lens that provides a magnified view for observation and photographs. The holographic filter would be placed in plane H, and then followed by further magnifying optics.

Figure 34 shows a photograph of our laboratory experimental setup. The experimental setup shown in Figure 34 has the following basic parameters. A one milliwatt fundamental transverse-mode helium-neon laser with wavelength $0.63 \mu\text{m}$ provides the light source. The ultrasonic point-source is formed by a one centimeter diameter quartz transducer crystal radiating into a 7 cm diameter, 7 cm radius-of-curvature glass mirror. The ultrasonic frequency is 5 MHz. The acoustic power is 0.25 watt. The water tank has two 10 by 10 cm windows, and is 10 cm wide. Lens (L_2) has a radius-of-curvature of 12 cm. Lens (L_3) is actually two 3-element lenses combined. Each has a focal length of 60 cm. Lenses (L_1) and (L_4) are twenty-power microscope objectives. The system operates with a diffraction-limited numerical aperture of 0.06 to 0.10 in water. This corresponds to a half-angle of from 3 to 6 degrees. This angle and the acoustic wavelength determine the ultimate resolution of the microscope. We hope to increase this angle in the future.

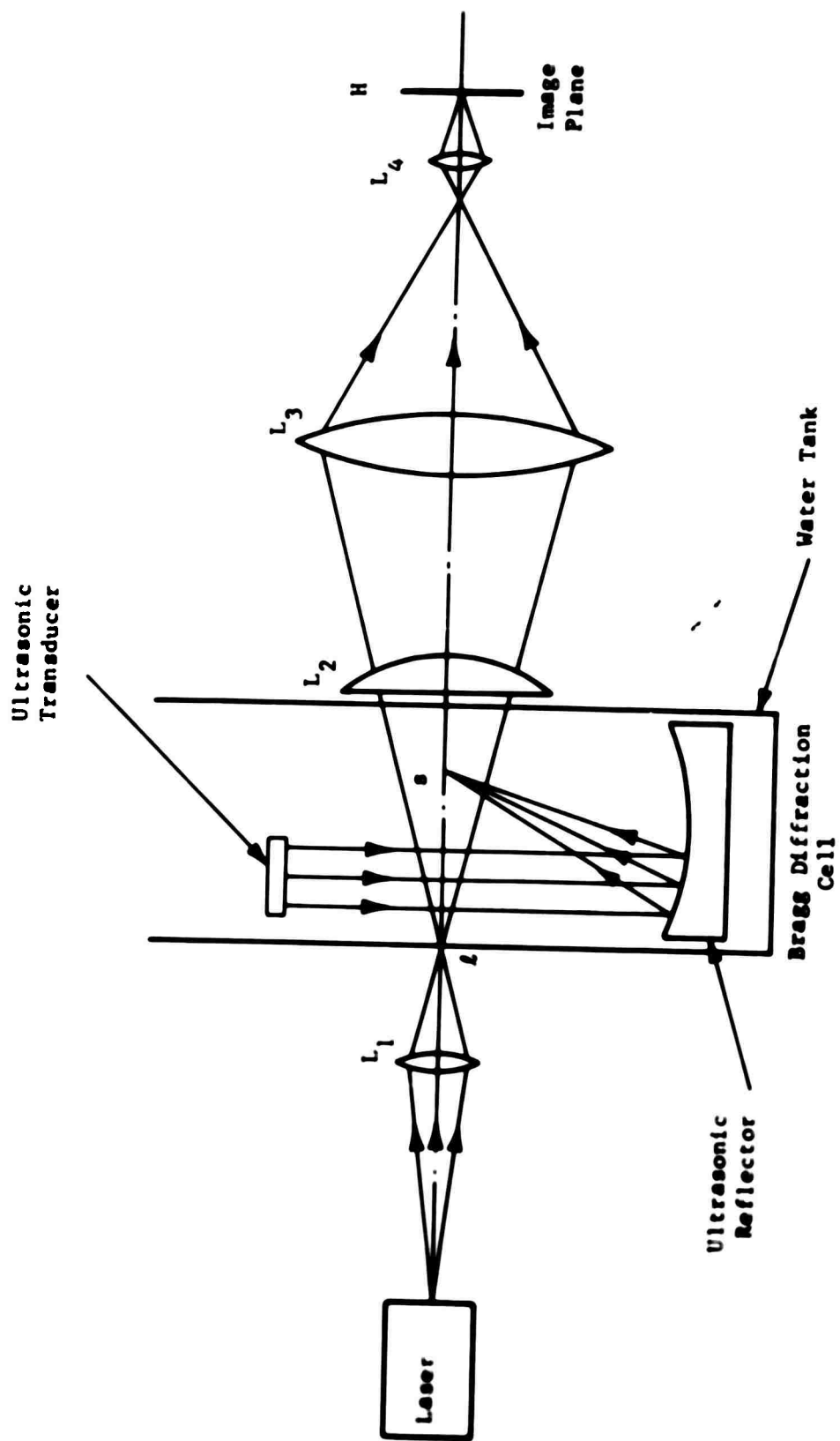


Figure 33. Schematic Diagram - Lens Ultrasonic Diffraction Microscope

Figure 35 is a photograph of the ring pattern produced by a point acoustic source on the optical axis. Only part of the diffraction ring image shows, because the acoustic point-source formed in the tank is not a true point-source emitting spherical waves, but only a small part of a spherical wave. Only sound rays with angles corresponding to the waves emitted by the one-centimeter diameter transducer are present.

After experimenting with the spherical lens system shown in Figure 33, the spherical mirror system shown in Figure 36 was designed as a more practical way of increasing the numerical aperture. Mirror M is a simple spherical mirror, whereas in Figure 33 Lens L_3 was a compound lens of 6 elements with aspheric surfaces. The lenses in Figure 36 function as the corresponding lettered lenses in Figure 33. The spherical mirror is located with its center-of-curvature at (L). Lens L_2 could be eliminated, if the mirror is placed in the cell, or made on the outer surface of the cell. The beamsplitter separates the incident and image (return) light beams.

Figure 37 shows our experimental mirror diffraction microscope with the diffraction ring in plane H. Lens L_4 is absent.

The spherical mirror diffraction microscope appears to allow us to use small cylindrical lens near L_1 and L_4 with a line source, as opposed to the large cylindrical lens required by the all-lens system. Thus, we will reconsider the cylindrical lens line-source system, and compare it to the spherical mirror system which uses the magnified holographic filter.

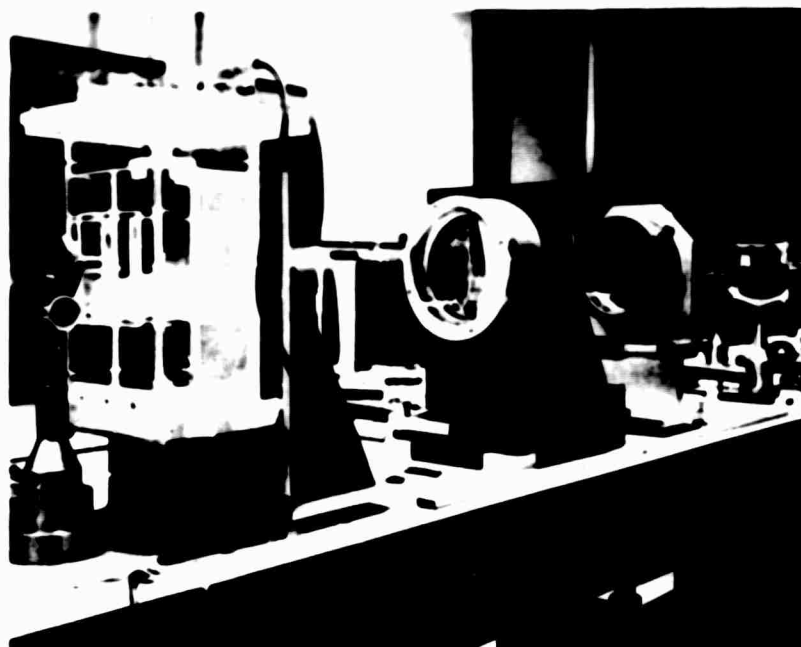


Figure 34. Photograph - Spherical Lens Ultrasonic Diffraction Microscope

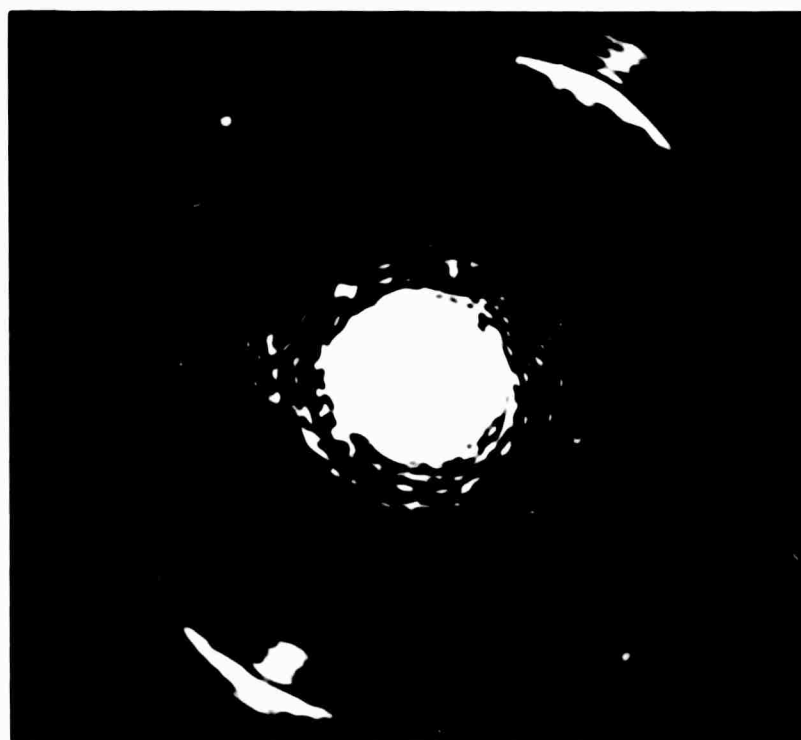


Figure 35 Light Intensity Distribution in Diffraction Plane of Ultrasonic Diffraction Microscope

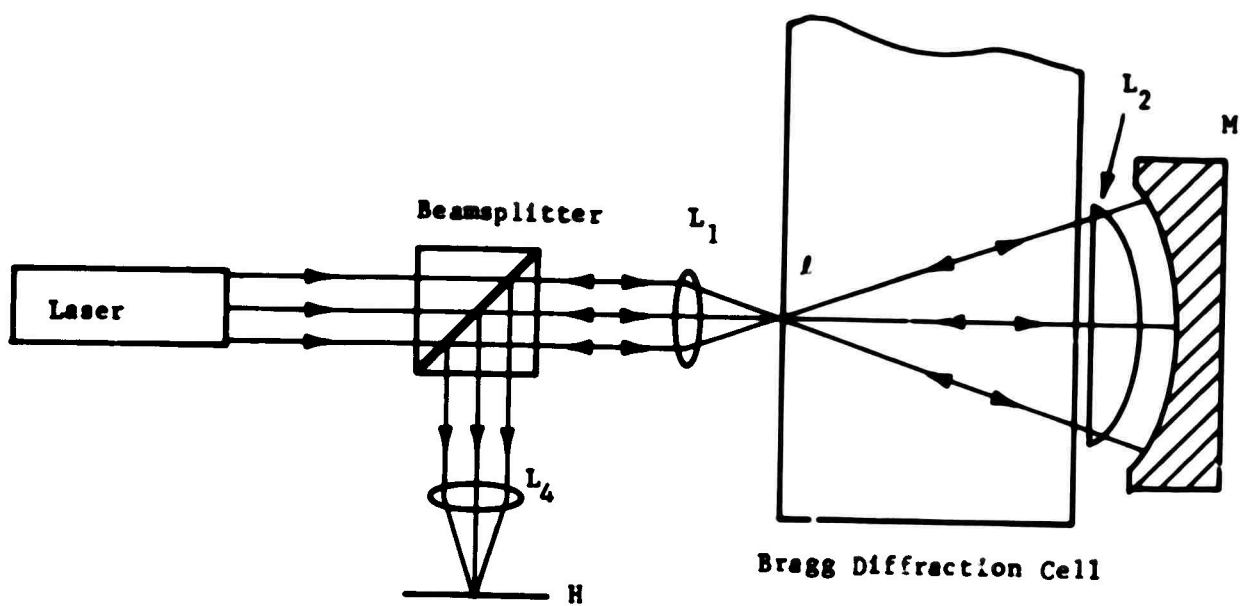


Figure 36. Schematic Diagram - Mirror Ultrasonic Diffraction Microscope

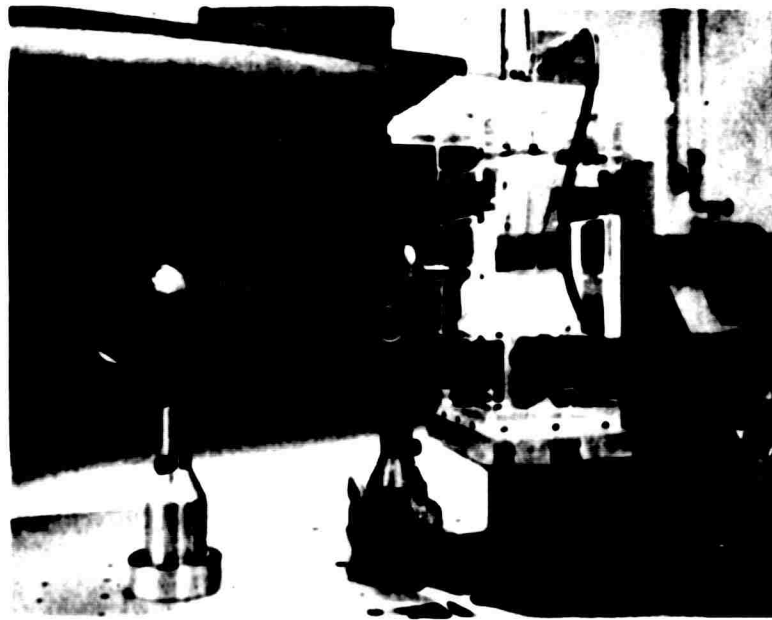


Figure 37. Photograph - Mirror Ultrasonic
Diffraction Microscope

REFERENCES

- ¹ Kreuzer, J.L., Proceedings of the Symposium on Modern Optics, Polytechnic Press, Vol. XVII, page 91 (March 1967).
- ² Kreuzer, J.L. and Vogel, P.E., Edited by Metherell, A.F., et al., Acoustical Holography, Plenum Press (1969).
- ³ Leith, E.N. and Upatnieks, J., JOSA (Oct. 1962).
- ⁴ Kreuzer, J.L. and Preston, K., Jr., Appl. Phys. Lett. (1 March 1967).
- ⁵ Preston, K., Jr., Photographic Science and Engineering, Volume 11, Number 3, May-June 1967.
- ⁶ Strong, J., Concepts of Classical Optics (1958).
- ⁷ Korpel, A., "Visualization of the Cross Section of a Sound Beam by Bragg Diffraction of Light," Applied Physics Letters, Vol. 9, No. 12, p. 425 (1966).
- ⁸ Korpel, A., "Acoustic Imaging by Diffracted Light 1. Two Dimensional Interaction," IEEE Transactions on Sonics and Ultrasonics, Vol. SU-15, No. 3, p. 153 (1966).
- ⁹ Tsai, Chen S., and Hance, A.V., "Optical Imaging of the Cross Section of a Microwave Acoustic Beam in Rutile by Bragg Diffraction of a Laser Beam," the Jour. of the Acoustical Society of America, Vol. 42, No. 6, p. 1345 (1967).
- ¹⁰ Landry, K., Powers, J., and Wade, G., "Ultrasonic Imaging of Internal Structure by Bragg Diffraction," Applied Physics Letters, Vol. 15, No. 6, p. 186 (1969).

UNCLASSIFIED

Security Classification

DOCUMENT CONTROL DATA - R & D

(Security classification of title, body of abstract and indexing annotation must be entered when the overall report is classified)

1. ORIGINATING ACTIVITY (Corporate author)

The Perkin-Elmer Corporation
Optical Group - Research
Norwalk, Connecticut 06897

2a. REPORT SECURITY CLASSIFICATION

Unclassified

2b. GROUP

3. REPORT TITLE

Investigation of the Application of Coherent
Acoustic Imaging to Nondestructive Testing

4. DESCRIPTIVE NOTES (Type of report and inclusive dates)

Semi-Annual Technical Report - May 1, 1969 to October 31, 1969

5. AUTHOR(S) (First name, middle initial, last name)

Walter R. Arndt
Justin L. Kreuzer

6. REPORT DATE

April 1970

7a. TOTAL NO OF PAGES

59

7b. NO OF REFS

10

8a. CONTRACT OR GRANT NO

Contract DAAG 46-69-C-0010

8b. ORIGINATOR'S REPORT NUMBER(S)

AMRC CR 70-14

9. PROJECT NO

9b. OTHER REPORT NO(S) (Any other numbers that may be assigned this report)

Parkin-Elmer**Engr. Rpt. No. 9725**

10. DISTRIBUTION STATEMENT

This document has been approved for public release and sale; its distribution is unlimited.

11. SUPPLEMENTARY NOTES

12. SPONSORING MILITARY ACTIVITY

Army Materials and Mechanics Research
Center, Watertown, Massachusetts 02172

13. ABSTRACT

The purpose of this research program is to analyze and perform experimental demonstrations of the application of ultrasonic holographic and ultrasonic light diffraction techniques to the detection, analysis, and examination of the internal structure of optically opaque materials. During the period covered by this report, the electronic circuits for the ultrasonic camera were redesigned and the new hardware fabricated and tested. The revised system, described in detail in this report, has the inherent flexibility improved stability, and enhanced performance to permit the accurate generation of ultrasonic holograms. An elementary theory of the ultrasonic diffraction microscope is outlined in the report and some preliminary supporting experiments are described.

DD FORM 1473REPLACES DD FORM 1473, 1 JAN 60 EDITION
GPO: 1969 O-355-96**UNCLASSIFIED**

Security Classification

1.6 KEY WORDS	LINE A		LINE B		LINE C	
	ROLE	BY	ROLE	BY	ROLE	BY
Nondestructive tests						
Holography						
Ultrasonic frequencies						
Lasers						
Diffraction						
Interferometers						
Optical interference						
Sound transmission						
Wave interference						